Published in final edited form as:
J Comp Neurol. 2006 July 20; 497(3): 326–349. doi:10.1002/cne.20970.

Central Projections of Melanopsin-Expressing Retinal Ganglion Cells in the Mouse

SAMER HATTAR[1], **MONICA KUMAR**[3], **ALEXANDER PARK**[1], **PATRICK TONG**[2], **JONATHAN TUNG**[3], **KING-WAI YAU**[1,2], and **DAVID M. BERSON**[3,*]

[1] Department of Neuroscience, Johns Hopkins University School of Medicine, Baltimore, Maryland 21205-2105

[2] Department of Ophthalmology, Johns Hopkins University School of Medicine, Baltimore, Maryland 21205-2105

[3] Department of Neuroscience, Brown University, Providence, Rhode Island 02912

Abstract

A rare type of ganglion cell in mammalian retina is directly photosensitive. These novel retinal photoreceptors express the photopigment melanopsin. They send axons directly to the suprachiasmatic nucleus (SCN), intergeniculate leaflet (IGL), and olivary pretectal nucleus (OPN), thereby contributing to photic synchronization of circadian rhythms and the pupillary light reflex. Here, we sought to characterize more fully the projections of these cells to the brain. By targeting *tau-lacZ* to the melanopsin gene locus in mice, ganglion cells that would normally express melanopsin were induced to express, instead, the marker enzyme β-galactosidase. Their axons were visualized by X-gal histochemistry or anti-β-galactosidase immunofluorescence. Established targets were confirmed, including the SCN, IGL, OPN, ventral division of the lateral geniculate nucleus (LGv), and preoptic area, but the overall projections were more widespread than previously recognized. Targets included the lateral nucleus, peri-supraoptic nucleus, and subparaventricular zone of the hypothalamus, medial amygdala, margin of the lateral habenula, posterior limitans nucleus, superior colliculus, and periaqueductal gray. There were also weak projections to the margins of the dorsal lateral geniculate nucleus. Co-staining with the cholera toxin B subunit to label all retinal afferents showed that melanopsin ganglion cells provide most of the retinal input to the SCN, IGL, and lateral habenula and much of that to the OPN, but that other ganglion cells do contribute at least some retinal input to these targets. Staining patterns after monocular enucleation revealed that the projections of these cells are overwhelmingly crossed except for the projection to the SCN, which is bilaterally symmetrical.

Indexing terms

melanopsin; circadian; retinofugal; pupil; suprachiasmatic nucleus; retinal ganglion cell; retinohypothalamic tract; pretectum; superior colliculus

Melanopsin is an opsin protein originally identified in frog dermal melanophores (Provencio et al., 1998, 2000) and now firmly established as a functional sensory photopigment (Newman et al., 2003; Melyan et al., 2005; Panda et al., 2005; Qiu et al., 2005; Fu et al., 2005). In mammals, it is expressed in the eye, almost exclusively in a small percentage of retinal ganglion

[*]Correspondence to: David M. Berson, Department of Neuroscience, Box 1953, Brown University, Providence, RI 02912. David_Berson@Brown.edu.
Dr. Hattar's current address: Department of Biology, Johns Hopkins University, Baltimore, MD 21218-2685.

cells (RGCs; Provencio et al., 2000, 2002; Hannibal et al., 2002; Hattar et al., 2002). These melanopsin-expressing RGCs (mRGCs) are directly sensitive to light and thus constitute a third class of mammalian retinal photoreceptors, in addition to the rods and cones (Berson et al., 2002; Berson, 2003; Warren et al., 2003).

Among their many striking structural and functional differences from the classical photoreceptors is that, as ganglion cells, they project directly to the brain. One target of these projections is the suprachiasmatic nucleus of the hypothalamus (Gooley et al., 2001; Berson et al., 2002; Hannibal et al., 2002; Hattar et al., 2002), a link that helps to synchronize this master pacemaker of circadian rhythms to the solar cycle (Berson, 2003; Hirota and Fukada, 2004). A second target, the intergeniculate leaflet (Hattar et al., 2002, Morin et al., 2003), also participates in circadian photoentrainment (Harrington, 1997). A third output reaches the olivary pretectal nucleus (Hattar et al., 2002; Morin et al., 2003), a key element in the circuit mediating the pupillary light reflex (Trejo and Cicerone, 1984; Clarke and Ikeda, 1985; Young and Lund, 1994).

Other targets of the mRGCs have begun to emerge, implying their participation in diverse functions. These targets include the preoptic region, hypothalamic subparaventricular zone, ventral lateral geniculate nucleus, and superior colliculus (Hattar et al., 2002; Gooley et al., 2003; Morin et al., 2003; Hannibal and Fahrenkrug, 2004). Past studies of these projections have relied mainly on retrograde transport of tracers injected into candidate targets combined with immunohistochemistry or in situ hybridization to identify retinal cells expressing melanopsin. This has limited the number of possible targets probed, and little information has been available about the form, trajectory, or distribution of the axons. In this study, we set out to describe the full extent of central projections of mRGCs, exploiting a gene-targeted mouse strain engineered to express the β-galactosidase marker enzyme selectively in mRGCs (Hattar et al., 2002).

A second goal of the present study was to characterize the relative strength of ipsilateral and contralateral projections from the mRGCs. A striking feature of the retinohypothalamic projection in the mouse is that the crossed and uncrossed components are about equally strong (Youngstrom and Nunez, 1986; Cassone et al., 1988; Miura et al., 1997; Abrahamson and Moore, 2001), whereas more than 95% of retinal fibers are crossed in the rest of the visual system (Drager and Olsen, 1980; Miura et al., 1997). Because most retinal afferents to the SCN are derived from mRGCs, we wondered whether these ganglion cells may also have unusually robust ipsilateral projections to their other targets. To pursue this issue, we examined in the same knock-in mice the effects of monocular enucleation on the relative density of β-galactosidase-positive fibers on the two sides of the brain.

We also sought further evidence on the degree to which inputs from mRGCs converged with those of other RGCs (non-mRGCs) in specific target nuclei. All photic responses to which mRGCs are known to contribute persist in some form when the melanopsin gene is knocked out (Panda et al., 2002; Ruby et al., 2002; Lucas et al., 2003; Mrosovsky and Hattar, 2003). Because direct photosensitivity is lost in mRGCs when melanopsin is deleted (Lucas et al., 2003), the residual responses presumably reflect the influences of rods and/or cones (Hattar et al., 2003; Panda et al., 2003). Indeed, there is electrophysiological evidence for rod and cone input to the SCN (Aggelopoulos and Meissl, 2000). The routes by which these rod/cone signals reach the critical brain nuclei are unknown. The mRGCs themselves are a likely conduit, because these cells are known to be excited by rod- or cone-driven synaptic networks (Dunn and Berson, 2002; Belenky et al., 2003; Dacey et al., 2005) and because they retain their normal axonal outputs in the face of melanopsin deletion (Lucas et al., 2003). Alternatively, conventional (non-melanopsin) ganglion cells may relay rod and cone signals to these brain regions (Gooley et al., 2001; Morin et al., 2003; Sollars et al., 2003; Hannibal and Fahrenkrug,

2004). We assessed the relative contribution of mRGCs and non-mRGCs to the retinal input to individual nuclei by double-immunofluorescence experiments in which antero-grade transport labeled all retinal afferents while β-galactosidase marked the axons of melanopsin RGCs.

MATERIALS AND METHODS

Animals

All procedures were conducted in accordance with NIH guidelines and approved by the Institutional Animal Care and Use Committees of Brown University and Johns Hopkins University. The studies used 24 male and female adult mice of the B6/129 strain genetically modified to replace the melanopsin gene *opn4* with *tau-lacZ* (Hattar et al., 2002). The *tau-lacZ* gene codes for a protein consisting of the β-galactosidase enzyme fused to a signal sequence from tau to promote axonal transport of the marker enzyme (Mombaerts et al., 1996). Except where specifically stated, all data are based on 22 mice that are homozygous for the tau-lacZ knock-in (*tau-lacZ*$^{+/+}$) and are therefore completely devoid of melanopsin (*opn4*$^{-/-}$). Animals were not backcrossed to an inbred strain. Animals were housed under a 14:10-hour light-dark cycle and were killed during the light phase.

X-gal labeling

To visualize the β-galactosidase marker enzyme, mice were anesthetized by intraperitoneal injection of tribromoethanol (Winthrop Laboratories, New York, NY) (0.2 ml/g) and arterially perfused for 10 minutes with 25 ml of cold 4% paraformaldehyde in phosphate-buffered saline (PBS; pH 7.4). Brains were removed, cryoprotected in 30% sucrose in PBS overnight, and cut coronally on a sliding microtome at 50 μm. X-gal staining followed Mombaerts et al. (1996). Sections were washed twice for 10 minutes each in buffer B (100 mM phosphate buffer at pH 7.4, 2 mM $MgCl_2$, 0.01% Na-desoxycholate, and 0.02% [octylphenoxy] polyethoxyethanol [IGEPAL]). They were then incubated in staining solution [buffer B plus potassium ferri-cyanide (5 mM), potassium ferrocyanide (5 mM), and X-gal[1] (5-bromo-4-chloro-3-indolyl-β-D-galactopyranoside; 1 mg/ml] at room temperature in darkness. Incubations lasted for 6 – 8 hours for homozygotes and 12–18 hours for heterozygotes. For retinal labeling, eyes were removed from animals, fixed as described above, and hemisected near the ora serrata. The lens and vitreous were removed, the remaining eyecup was stained with X-gal as above for 24 –30 hours at 37°C in darkness, and the retina was isolated. Retinas and brain sections were mounted on glass slides and coverslipped in glycerol. For X-gal staining of whole brains, animals were perfused first with fixative, as above, and then with 60 ml of the X-gal staining solution. The brain was then removed and immersed in the same staining solution for 3–5 days at 36°C. The brain was dehydrated and cleared by immersion in methanol (2 days) and then in a 2:1 solution of benzyl benzoate and benzyl alcohol (2 hours) and then immersed in light mineral oil for photography.

Enucleation

A total of seven mice were subjected to monocular (n = 6) or binocular (n = 1) enucleation. They were anesthetized by intramuscular ketamine (50 mg/kg ip), and the eyes were topically anesthetized with a drop of 0.5% tetracaine (Wilson Ophthalmics, Mustang, OK). One or both eyes were proptosed by gentle lid retraction and enucleated with Vannas scissors. Pressure applied with cotton gauze provided hemostasis. The mice were placed in a warm chamber (37° C) for 1 hour during recovery from anesthesia. Mice were sacrificed 15–21 days after the enucleation.

[1]X-gal is from VWR, Bridgeport, NJ. All other reagents are from Sigma (St. Louis), unless otherwise stated.

Cholera toxin tracing experiments

Mice were anesthetized with ketamine (60 mg/kg ip) and medetomidine (1.0 mg/kg ip) and placed in a stereotaxic device. One eye was incised just behind the ora serrata with a 30G hypodermic needle and injected intravitreally with cholera toxin B subunit (CTB; 1 μl of a 1% w/v solution in distilled water) either in the unconjugated form (List Biological Lab., Campbell, CA; polyclonal) or conjugated to Alexa Fluor 488 (C-22841; Molecular Probes, Eugene, OR). For the data shown in Figure 9F–J, the CTB injection was binocular but failed in one eye, producing negligible anterograde labeling, so that the overall labeling pattern was effectively like that in cases of monocular injection. Anesthesia was then reversed with atipamezole (2 mg/kg ip; Pfizer, Exton, PA). Three days after surgery, mice were killed with an overdose of Nembutal and perfused transcardially with PBS followed by 4% paraformaldehyde in PBS. The brain was placed in the same fixative for 1 hour and then cryoprotected overnight in 30% sucrose in PBS.

Single- and double-label immunofluorescence processing

For all immunohistochemical studies, coronal sections of the brain were cut as for the X-gal studies, washed (3 × 5 minutes) in PBS, and blocked with 6% normal donkey serum (NDS) in PBS containing 0.3% Triton X-100. For double-immunofluorescence visualization of CTB and β-galactosidase, sections were incubated (72 hours; 4°C) in a mixture of the two primary antibodies, a polyclonal goat anti-choleragenoid antibody (List #703, 1:5,000) and a polyclonal rabbit antibody raised against highly purified β-galactosidase from *E. coli* [Cortex (San Leandra, CA) #CR7001RP5, 1:2,000], containing 0.3% Triton X-100 and 2% NDS. Sections were washed in PBS, incubated in Alexa-488-tagged donkey anti-rabbit secondary antibody (Molecular Probes A-21206, 1:400), washed again, and incubated in Alexa-568-tagged donkey anti-goat secondary (Molecular Probes A-11057, 1:400). When CTB was visualized instead by direct conjugation to Alexa 488 (see above), β-galactosidase immunofluorescence was achieved with a polyclonal rabbit anti-β-galactosidase primary antibody (Eppendorf-5 Prime, Boulder, CO; 1:1,000; overnight at 4°C) and a goat anti-rabbit secondary antibody tagged with Alexa 568 (Molecular Probes, A11011; 1:400). Secondary antibody solutions included 0.3% Triton X-100 and 2% NDS, and incubations were carried out for 1–2 hours at room temperature. Sections were washed, mounted on glass slides, and coverslipped with Vectashield (Vector, Burlingame, CA).

Anti-CTB immunolabeling was evident only in known retinofugal tracts or targets, matched the distribution of transported CTB directly tagged with Alexa488, and was absent in brains from mice not injected with the tracer. Anti-β-galactosidase immunoreactivity with either antibody corresponded closely to the pattern of histochemical staining for the enzyme by X-gal and was undetectable in wild-type brains. For anti-VIP immunofluorescence, we followed Abrahamson and Moore (2001), using the same primary antibody [Immunostar (Hudson, WI) polyclonal rabbit anti-VIP IgG raised against porcine VIP conjugated to bovine thyroglobulin, #20077; 1:20,000], but substituting the Alexa-488-labeled donkey anti-rabbit secondary antibody described above (Molecular Probes). The distribution of VIP-like immunofluorescence in the SCN closely matched earlier descriptions (Abrahamson and Moore, 2001). Such immunostaining is abolished by preadsorption with VIP but not with various other neuropeptides (manufacturer's technical information).

A few retinas were immunostained for β-galactosidase. Retinas were postfixed overnight in 4% paraformaldehyde (in PBS) at 4°C. Immunohistochemical protocols followed those used for the brain sections except that the anti-β-galactosidase primary antibody (Cortex #CR7001RP5) was used at 1:1,000 dilution and the secondary antibody was tagged with Alexa Fluor 488, used at 1:250 dilution, overnight at 4°C.

Microscopy and image processing

Brightfield images of X-gal staining and epifluorescence images of immunostaining were acquired on a Nikon E-600 compound microscope equipped with a 100-W mercury arc lamp and a Spot RT Slider camera (Diagnostics Instruments; Sterling Heights, MI) coupled to a Dell Pentium III computer running Windows 2000 and SPOT software. Confocal images were obtained at 16-bit resolution on a Zeiss 410 laser scanning microscope by using a krypton-argon laser. Images acquired were imported into Adobe (San Jose, CA) Photoshop 6.0, and global adjustments were made to optimize brightness and contrast. In some cases, depth of field was enhanced in Photoshop by selectively masking portions of each image in a stack of images obtained at a series of focal planes so as to display only those portions of each image in which the labeled elements were in optimal focus. For double immunofluorescence, care was taken in making adjustment of sensitivity to ensure separation of the signals from the two fluorophores. Except where noted, boundaries and full names of nuclei follow the atlas of Paxinos and Franklin (2001), although some abbreviations have been changed for consistency with those widely used in the literature on non-image-forming visual networks. The plates of that atlas also served as the model for the schematic coronal sections of Figure 4.

RESULTS

The distribution and form of β-galactosidase-positive cells and processes were virtually identical whether visualized by X-gal staining or by anti-β-galactosidase immunofluorescence. The marker enzyme was detectable only in a small population of inner retinal neurons and in their axons in the optic pathway. No β-galactosidase-positive somata were observed anywhere in the brain, and axonal labeling in the brain was abolished by binocular enucleation (data not shown). The β-galactosidase-positive fibers were essentially restricted to a subset of targets within the overall retinofugal projection as revealed by CTB labeling, although the superior signal-to-noise properties of the β-galactosidase methods permitted detection of isolated fibers and sparse terminal fields that could have been missed had we relied on the CTB method alone. Thus, we conclude that all axons labeled by X-gal histochemistry or anti-beta galactosidase immunostaining derive from retinal ganglion cells that would normally express melanopsin (mRGCs).

Retina

Labeled cell bodies were observed exclusively in the inner retina. The great majority occupied the ganglion cell layer, but roughly 5% lay in the inner nuclear layer near its inner border. The latter were presumably displaced ganglion cells rather than amacrine cells, because when they were well stained, their axons could be traced into the optic fiber layer. In well-stained material, approximately 750 cells in each retina were X-gal positive. These were distributed relatively uniformly over the retina, although in some retinas there appeared to be an elevated density of cells at the retinal margin (Fig. 1, inset). The extent of dendritic labeling was highly variable both within and among retinas. In the best stained cells, dendrites could be followed for several hundred micrometers (Fig. 1), and these invariably arborized within the outermost stratum of the IPL, adjacent to the inner nuclear layer. With few exceptions, labeled axons could be seen emerging from well-stained cells and coursing toward the optic disk (Fig. 1, arrowheads).

Optic nerve and tract

Labeled fibers were distributed throughout the optic nerve as it approached the chiasm. Figure 2A illustrates a confocal image of a transverse cross section of the nerve immunostained for β-galactosidase. A total of 777 labeled axons were counted in this section, which corresponds closely to the counts of X-gal-labeled somas in the retina. Beyond the optic chiasm, X-gal positive fibers became clearly segregated within the optic tract, occupying mainly the periphery of the tract's dorsal half and largely avoiding its core or ventral aspect (Fig. 2C). After

monocular enucleation, nearly all X-gal-positive fibers in the contralateral optic tract degenerated, leaving only weakly stained granular debris (Fig. 2B) and a smattering of intact labeled axons, which presumably arose from the intact ipsilateral eye. A complementary pattern was evident in the tract ipsilateral to the enucleation (Fig. 2C), with very little evidence of degenerating labeled fibers. Thus, beyond the hypothalamus, the projections of mRGCs are overwhelmingly crossed.

Overview of projections to the brain

The distributions of labeled fibers were highly consistent from brain to brain, whether visualized by X-gal staining or anti-β-galactosidase immunofluorescence, although the sparser terminal fields were sometimes undetectable in cases of suboptimal staining. An overview of the central projections of these RGCs appears in Figures 3 and 4. Figure 3 shows the trajectories and terminations of X-gal-stained fibers in a stained brain wholemount, viewed from its dorsal (Fig. 3A) or lateral (Fig. 3B) aspect. The most prominent targets are summarized in the schematic diagram of Figure 3C. Figure 4 illustrates the distribution of labeled fibers after monocular (right) enucleation in schematic chartings of coronal sections and thus provides an indication of the relative weighting of crossed and uncrossed projections from these ganglion cells to specific brain nuclei.

Several major regions of termination are apparent in these figures. The first lies near the optic chiasm and includes not only the dense projections to the suprachiasmatic nucleus but also several other hypothalamic nuclei and the amygdala. The second lies in and near the lateral geniculate complex and can be traced rostrally as far as the vicinity of the anterior thalamic nuclei and bed nucleus of the stria terminalis. Fibers pass medially from the geniculate complex and course over the dorsal surface of the brain to innervate a third, chevron-shaped terminal zone, the rostral arm of which abuts the habenula. The other arm runs caudolaterally along the pretectothalamic border in what may be the posterior limitans nucleus. Just caudal to this, a fourth, very dense terminal field marks the olivary pretectal nucleus, and sparser terminations are also apparent in the superior colliculus and periaqueductal gray.

There was a marked difference in appearance between passing fibers, such as those in the optic tract, and fibers in presumed terminal zones. Passing fibers were generally very thin, relatively straight, sparsely varicose, and more lightly stained, whereas those in terminal zones appeared thicker and more densely stained. When fiber density was low enough to resolve individual fibers, they appeared tortuous and often exhibited branching and prominent terminal swellings.

Suprachiasmatic nucleus

The SCN is the most densely innervated target of β-galactosidase-positive fibers in these mice. After monocular enucleation, labeling was remarkably bilaterally symmetric, indicating that mRGCs in each eye projects equally strongly to the two SCNs (Figs. 4, 5A). In double-immunofluorescence experiments, most CTB-labeled retinal afferents in the SCN (red) were also β-galactosidase immunopositive (green), so most retinal afferents to this nucleus apparently arise from mRGCs (Fig. 5B–E). However, at least a few CTB-positive fibers and puncta lacked β-galactosidase (filled arrows in Figs. 5D,E), and these presumably arose from non-mRGCs. X-gal-positive fibers appeared to fill the entire nucleus including both its “shell” and “core” subregions, as defined either cytoarchitecturally or by the distribution of fibers immunoreactive for vasoactive intestinal peptide (VIP; Abrahamson and Moore, 2001;Yan and Silver, 2002; Fig. 5F–I).

Other hypothalamic and basal limbic targets

Labeled fibers were present in a variety of hypothalamic nuclei in addition to the SCN. Rostrolateral to the SCN, scattered fibers reached the lateral and ventrolateral preoptic area

and in some brains encroached on the nucleus of the horizontal limb of the diagonal band (Fig. 4, sections 1 and 2; Fig. 6A,B). Fibers extended dorsally and caudally from the SCN to infiltrate the ventral part of the subparaventricular zone (vSPZ; Lu et al., 2001; Fig. 5H). These were almost entirely limited to the ventral part of the vSPZ as defined by the distribution of VIP-immunoreactive fibers (Fig. 5H,I), whereas the dorsal SPZ and paraventricular nucleus were essentially devoid of labeling. Double-immunofluorescence material indicated that the majority of retinal afferents in the vSPZ come from mRGCs (Fig. 6D–F) but that at least some appear to originate in non-mRGCs. Monocular enucleation revealed that the uncrossed input from mRGCs to this region is nearly as strong as the crossed input (Fig. 5A).

Labeled fibers coursed dorsally and laterally from the SCN to weakly innervate the lateroanterior hypothalamic and medial preoptic nuclei. There was relatively dense fiber labeling in the retrochiasmatic region, including parts of the lateroanterior nucleus and central division of the anterior hypothalamic nucleus (Fig. 4, sections 7 and 8; Fig. 6C). This labeling was continuous with that in the vSPZ and may lie within the caudal part of the SPZ (Lu et al., 2001). As the optic tract emerged from the optic chiasm, fibers peeled off dorsally to form a moderately dense nest in the vicinity of the supraoptic nucleus (SON; Fig. 4, sections 5–7; Fig. 6A,C). Most of these fibers appeared to terminate just dorsal to the nucleus itself, in a region that has been termed the peri-supraoptic nucleus (pSON). Double-immunofluorescence material revealed that substantial numbers of CTB-labeled retinal afferents in this region lacked β-galactosidase and thus presumably originate from non-mRGCs (data not shown). In well-stained brains, a few β-galactosidase-positive fibers could be seen innervating the medial amygdaloid nucleus (Fig. 4, section 8; Fig. 6C). One or two labeled fibers were also detected in the zona incerta and substantia innominata in some brains.

We scanned the piriform cortex with particular care because this region is sparsely innervated by retinal fibers in rodents and primates (Pickard and Silverman, 1981; Mick et al., 1993; Ling et al., 1998) and because in mice with advanced degeneration of rods and cones light evokes biochemical responses in this region (Alvarez-Lopez et al., 2004), suggesting a possible input from mRGCs. However, neither β-galactosidase-positive fibers nor CTB-labeled retinal afferents were observed in this region in any brain. Other than the SCN and vSPZ, all the basal limbic nuclei appeared to have stronger mRGC input from the contralateral retina than from the ipsilateral retina, although all these regions appeared to receive at least a weak uncrossed retinal input.

Intergeniculate leaflet

Beyond the amygdala, labeled fibers coursed within the optic tract without obvious terminations until they reached the lateral geniculate complex. By far the densest terminal labeling within the geniculate complex was in the intergeniculate leaflet (IGL; Figs. 3A, 7, 9). In coronal sections through most of the length of the geniculate complex, this zone of dense labeling corresponded closely to the IGL as shown in the atlas of Paxinos and Franklin (2001), a thin band separating the dorsal and ventral divisions of the lateral geniculate nucleus (LGd and LGv). However, this distinctively dense plexus of labeled fibers continued both rostrally and caudally beyond the confines of the IGL as shown in the atlas. Because this comports with the extent of the nucleus as revealed by other markers for the IGL in rodents (Morin et al., 1992), we interpret the entire zone of dense fiber labeling as the IGL, departing in this respect from the Paxinos and Franklin atlas. Caudally, the IGL thus defined is found nearly as far back as the caudal pole of the medial geniculate nucleus. There, labeling consisted of a small group of fibers nestled between the dorsolateral margin of the cerebral peduncle, the caudalmost part of the optic tract, and the medial geniculate (Fig. 9D; see also Fig. 4, section 18), in a region termed the parapeduncular nucleus by Paxinos and Franklin (2001).

Rarely, fibers could be detected in the adjacent part of the zona incerta. Rostrally, the labeling in the IGL extended at least as far as the rostral pole of the LGd (Fig. 7B). Indeed, fibers in this terminal field extended still farther forward, albeit thinning progressively, where they occupied the dorsolateral margin of the dorsal thalamus at the level of the lateral dorsal thalamic nucleus, just dorsomedial to the stria terminalis (Figs. 3A,B, 4, sections 8 –10). In optimally stained brains, at least a few fibers could be traced nearly to the rostral pole of the dorsal thalamus, at which point they turned ventrally to end in the vicinity of the bed nucleus of the stria terminalis and anterior thalamic nuclei (Fig. 4, sections 4 and 5; Fig. 7C).

Monocular enucleation showed that ipsilateral-eye inputs from mRGCs to the IGL were far weaker than contralateral-eye inputs (Fig. 7A,D). The ipsilateral inputs were present to some degree throughout the IGL but tended to be heaviest in the dorsolateral half of the nucleus. Double-immunofluorescence staining showed abundant co-localization of β-galactosidase and CTB tracer in retinal afferents to the IGL (Fig. 7E,F), suggesting that most retinal inputs to this nucleus arise from mRGCs. However, at least some β-galactosidase-negative retinal terminals were apparent in the IGL both contralateral and ipsilateral to the monocular tracer injection (red puncta in Fig. 7E,F).

Ventral lateral geniculate nucleus

The most conspicuous terminal labeling in the LGv was found in a compact part of the parvocellular division. This was found ventromedially in the caudal part of the nucleus and was directly contiguous with the dense labeling of the IGL (Fig. 7A). In fact, in some brains, at least part of this terminal field appeared to be a small rostral extension of the caudoventral IGL. Tortuous fibers with apparent terminal swellings were scattered throughout the LGv, especially rostrally and medially in the parvocellular divisions, but these were far sparser than in the IGL. Elsewhere within the LGv, including within the external division, which is the most prominent target of retinal input, many of the labeled fibers were thin, took relatively straight, parallel courses, and lacked extensive branching or swelling. They thus appeared to be passing fibers en route to the IGL and more medial diencephalic regions. Enucleation experiments showed that the great bulk of the melanopsin RGC input to the LGv derives from the contralateral eye (Fig. 4, sections 13–17). Double-immunofluorescence analysis indicated that even the stronger crossed input from mRGCs accounts for only a small fraction of the overall retinal input to the LGv (Fig. 7E).

Dorsal lateral geniculate nucleus

Cursory examination revealed little obvious terminal labeling within the dorsal division of the lateral geniculate nucleus (LGd). Much of the nucleus was entirely devoid of fiber labeling, and the few readily discerned labeled axons appeared to be passing fibers (Fig. 7A, white arrow). These fibers, presumably constituents of the fascicles of the “internal optic tract” (see, e.g., Frost et al., 1986), paralleled those in the overlying optic tract and appeared to be heading for more medial targets such as the pretectal region and the habenula. In optimally stained brains, however, a thin sheet of sparse, tortuous fibers with apparent terminal swellings could be detected at the ventro-medial and rostral margins of the LGd. From examination of double-labeled material, it is clear that these fibers lie within the LGd proper as defined by dense, CTB-labeled retinogeniculate input. In coronal sections through the middle of the LGd, this sheet of terminal labeling appeared as a thin band paralleling the external medullary lamina. This terminal field was apparent not only in the crossed projection of mRGCs (Fig. 7A, black arrow) but also in the ipsilateral projection (Fig. 7D, black arrow), which appeared to terminate within the main ipsilateral-eye segment of the LGd. This band of labeling could be followed to the rostral pole of the LGd, where it curled upward so that it occupied the full cross section of the nucleus at this level (Fig. 7B; see also Fig. 3A,B).

Habenular region and posterior limitans nucleus

Labeled fibers coursed medially over the LGd in the superficial optic tract to terminate in a chevron-shaped field near the habenular complex and rostral border of the pretectum. The form of this terminal plexus is best appreciated in the dorsal view of the X-gal-reacted wholemount (Fig. 3A). The caudal arm of this field occupied the rostro-dorsal margin of the pretectal region, at its boundary with the dorsal thalamus (Fig. 4, sections 13 and 14). In coronal sections, this zone of labeling was visible at the dorsal surface of the anterior pretectal nucleus, where labeled axons of the superficial optic tract took on the darker, thicker appearance typical of terminal fibers (Fig. 8B). This region is considered an extension of the posterior limitans nucleus (PLi) in some rodents (e.g., Morin and Blanchard, 1997), and though this is not consistent with the mouse atlas of Paxinos and Franklin (2001), we tentatively adopt that nomenclature here. The main body of the rodent PLi is generally depicted as a thin shell abutting the lateral margin of the anterior pretectal nucleus. We were able to trace a very few β-galactosidase-positive axons to this region. These lay rostral to the PLi as drawn by Paxinos and Franklin (2001) and within what they consider the mediorostral division of the lateral posterior nucleus.

At the level of the habenular commissure, the terminal field assumed a purely rostrocaudal orientation (Fig. 3A), forming a very dense terminal plexus at the dorsolateral margin of the lateral habenular nucleus. This plexus lay in a cell-sparse region on the surface of the diencephalon, in the shallow groove where the habenula abuts the central lateral nucleus and lateral nuclear group of the thalamus (Figs. 3A, 4, sections 10 –12; Fig. 8A). The plexus was most prominent at the caudal end of the habenular complex and contained progressively fewer axons at more rostral levels. Nonetheless, it was readily apparent in most brains at least as far rostral as the rostral pole of the LGd, and in some brains an isolated fiber or two could be traced to the rostral limit of the habenula, just lateral to the stria medullaris. Although most of the fibers in this plexus lay within about 100 μm of the surface, a few fibers penetrated more deeply. These terminated at the lateral or, rarely, the ventral margins of the lateral habenula, within the fiber capsule that bounds the nucleus (Fig. 8A, arrowheads). Labeled fibers were sometimes found in association with the stria medullaris, but they never invaded the core of the lateral habenula. Nearly all CTB-labeled optic afferents in this region were β-galactosidase positive, indicating that melanopsin ganglion cells provide nearly all retinal input to this area (data not shown). These fibers were almost entirely crossed, although there is an extremely sparse ipsilateral input, as indicated by the one or two labeled fibers still evident contralateral to a removed eye (Fig. 4, section 12). Because mRGCs are presumed to exert substantial influence over the release of melatonin, we carefully examined the region of the pineal stalk and the pineal itself, but we observed no labeling in either structure.

Pretectal region

Except for the labeling in the posterior limitans nucleus, noted above, labeling in the pretectal region was almost entirely confined to a dense, well-defined terminal field that we consider to be the olivary pretectal nucleus (OPN; Fig. 4, sections 15–20). The terminal field was complex in shape, with a large, hollow head rostromedially and a tapering body that extended caudolaterally and typically split into two or three tails. Its rostral pole was found slightly behind the habenular commissure and just under the pial surface at the medial edge of the pretectal region (Fig. 9A). Here, it was ovoid in coronal cross-section and about 400 μm across. Although it lay fairly close to the caudal end of the terminal field in the posterior limitans nucleus, it was clearly separated from the PLi by a short span containing only passing fibers (Fig. 3A). Near the rostral pole, the terminal zone appeared hollowed out, taking on the form of an annulus in coronal sections (Fig. 9A,B,F,I). Caudally, the nucleus became horizontally elongated (roughly 300 μm wide and 50 –100 μm thick) and in some sections appeared to be broken into two or three patches (Figs. 3A, 9C,D,H,J). Most of these were elongated parallel to the tectal surface, 100 –200 μm in width, and were separated by largely terminal-free gaps

of about the same size. At more caudal levels, the terminal labeling assumed a progressively more lateral and ventral position, terminating near the dorsal terminal nucleus (DTN) of the accessory optic system.

Although rostrally this terminal zone corresponded closely to the olivary pretectal nucleus as defined by Paxinos and Franklin (2001), caudally it extended well beyond their OPN to encroach on what they designate as the caudal part of the posterior pretectal nucleus and the rostrolateral portions of the superior colliculus (stratum opticum and stratum griseum intermediale). The field of mRGC terminations corresponds more closely to the description of the anterior olivary pretectal nucleus of Pak et al. (1987), which they defined in wild-type mice on the basis of retinal input. However, the correspondence is imperfect because near the rostral pole of the nucleus, mRGC input was limited to a shell marking the margins of the circular field of overall retinal input (Fig. 9F,I). More caudally, the terminations of mRGCs lay at the base of the much broader zone of retinopretectal terminations that includes the nucleus of the optic tract and posterior pretectal nucleus (Fig. 9G,H,J; Scalia, 1972; Scalia and Arango, 1979; Pak et al., 1987). At its caudal limit, the mRGC terminal field lay just beneath the DTN. The DTN itself was generally devoid of mRGC axons, although a stray fiber or two could be detected in the best stained brains. The small nest of retinal input in the caudomedial pretectum that Pak et al. (1987) termed the posterior olivary pretectal nucleus was clearly evident in our CTB material (Fig. 9G) but apparently lacked any input from mRGCs.

The uncrossed input to the OPN from melanopsin RGCs was much weaker than the crossed input, as reported for other rodents (Muscat et al., 2003; Hannibal and Fahrenkrug, 2004) and appeared more restricted in its distribution (Fig. 9O), being essentially absent from the caudal third of the terminal field and from its ventral half at rostral levels. Double-immunofluorescence studies showed that even within the zone of densest termination of mRGC axons, many retinal terminals lacked the β-galactosidase marker enzyme and thus arose from non-mRGCs (Fig. 9K–N).

A small number of X-gal-labeled fibers coursed ventro-medially from the OPN toward the posterior commissure (Fig. 9O). Some penetrated the commissure itself, running perpendicular to its fibers, and could be traced into the underlying rostral periaqueductal gray. Others appeared to terminate more laterally, in and near the nucleus of the posterior commissure. This retinal terminal field appears to correspond to the commissural pretectal area in the rat (Prichard et al., 2002) and to the commissural pretectal nucleus in hamsters (Morin and Blanchard, 1997,1999). Very rarely, a few fibers could be traced caudally from this system as far as the periaqueductal gray beneath the caudal superior colliculus and to the vicinity of the dorsal raphe nucleus.

Superior colliculus

The superior colliculus was a significant target of labeled axons (Fig. 3A). These appeared to reach the SC primarily through the medial part of the brachium of the superior colliculus, passing caudally from the terminal field in the OPN. The fibers continued caudally in the stratum opticum of the SC, giving off dorsally directed branches at every coronal level through the nucleus. These represented a tiny fraction of overall retinal input to the SC (data not shown), and the sparseness of the fiber labeling made it possible to observe the morphology of individual fibers in considerable detail. Extensive branching, looping, and terminal swelling were seen in the superficial gray layer, and branches were often seen ascending as far as the stratum zonale, where they terminated just beneath the pia (Fig. 10). We rarely observed extensive clusters of terminal boutons on single axons, but when we did these could appear either in the upper or lower part of the superficial gray layer. In one brain, we detected two labeled axonal branches in the deeper collicular layers and underlying tegmentum.

Crossed projections to the tectum were much more prominent than uncrossed ones. Both crossed and un-crossed inputs were typically densest in the medial half of the SC, followed by its lateral margin (Fig. 10A), and were present throughout the rostrocaudal extent of the nucleus (Figs. 3A, 10C). The ipsilateral input was not confined to the deeper part of the superficial layers, as has generally reported for overall uncrossed retinal input (Godement et al., 1984), but instead clearly invaded the upper superficial gray layer and even reached the pial surface in some sections (Fig. 10C).

Lack of terminations in accessory optic system

All components of the accessory optic system were easily identifiable on the basis of their CTB-labeled retinal input. Labeling was entirely absent within the medial terminal nucleus, by far the largest accessory optic nucleus in the mouse (Pak et al., 1987). The lateral terminal nuclei (LTN) and inferior and superior fasciculi of the accessory optic tract were also devoid of β-galactosidase-positive fibers. Although labeled fibers terminating in the caudal pole of the OPN approached the ventral margin of the DTN, the DTN itself was typically free of labeling.

DISCUSSION

This study builds on recent work detailing the brain regions contacted directly by the axons of melanopsin-expressing, intrinsically photosensitive retinal ganglion cells (Gooley et al., 2001, 2003; Hannibal et al., 2002, 2004; Hattar et al., 2002; Morin et al.. 2003; Sollars et al., 2003; Dacey et al., 2005). The findings expand the range of target structures to include a diverse set of nuclei in the hypothalamus and other subcortical forebrain limbic zones, several divisions of the lateral geniculate complex, the habenular region, the superior colliculus, and the periaqueductal gray. Crossed inputs from mRGCs to these regions greatly outnumber uncrossed inputs except in the SCN and vSPZ, which get balanced inputs from the two eyes. Nearly all these terminal fields receive at least some input from RGCs that do not express melanopsin, although mRGCs appear to provide the dominant input to the SCN, IGL, and habenular region.

Anatomical and functional identity of mRGCs: are there multiple types?

There is no doubt that the fiber projections described here arise from retinal ganglion cells that normally express melanopsin. The retina was the only part of the central nervous system that contained β-galactosidase-positive somata. Furthermore, all β-galactosidase-containing axons in the brain could be traced back to the optic pathway, and all of them degenerated after bilateral eye removal.

Most, if not all, of these ganglion cells are presumably of the type shown to be intrinsically photosensitive (Berson et al., 2002), because these cells express melanopsin (Hattar et al., 2002; Dacey et al., 2005) and require it for their intrinsic photosensitivity (Lucas et al., 2003). The morphology of intrinsically photosensitive RGCs (Berson et al., 2002; Warren et al., 2003) closely matches that of cells expressing melanopsin in wild-type rodents (Hattar et al., 2002; Provencio et al., 2002; Hannibal et al., 2002) or expressing β-galactosidase in this study, especially in their predominant dendritic stratification in the outer-most IPL. Two of the densest projections evident in the present data, those to the SCN and OPN, have been directly confirmed for photosensitive ganglion cells in studies combining retrograde transport and intracellular recording (Berson et al., 2002; Dacey et al., 2005). Together, these data support the view that inputs from ganglion-cell photoreceptors sustain photic effects on circadian phase and pupil diameter in mice lacking functional rods and cones (Yoshimura and Ebihara, 1996; Lucas et al., 2001; Hattar et al., 2003). That view is further supported by the correspondence in spectral tuning among these residual behavioral photoresponses, the intrinsic light responses

of photosensitive ganglion cells, and the light responses of cells heterologously expressing melanopsin (Panda et al., 2005; Qiu et al., 2005; but see Melyan et al., 2005).

Although it is thus reasonable to conclude that most β-galactosidase-positive fibers in this study arise from intrinsically photosensitive RGCs, it is not certain that all do because there is some evidence for a second type of melanopsin-expressing ganglion cell. In the mouse retina, a sensitive melanopsin antibody (UF006) labels two tiers of immunopositive dendrites in the IPL (Provencio et al., 2002). Of these, only the outer tier, lying adjacent to the inner nuclear layer, matches the stratification of identified ipRGCs in rats (Berson et al., 2002; but see Warren et al., 2003). The second tier of melanopsin-immunopositive dendrites lies near the inner border of the IPL, close to the ganglion cells. These dendrites appear to arise from a second population of more weakly melanopsin-immunoreactive RGCs, with somewhat more radiate, orderly dendritic arbors (A. Castrucci, I. Provencio, and D. Berson, unpublished observations). This second population of immunoreactive RGCs has been termed M2 cells to distinguish them from the heavily stained M1 cells, which correspond to the ipRGCs. There are roughly equal numbers of M1 and M2 cells. Nothing is currently known about whether the M2 cells are intrinsically photosensitive or where they project in the brain. However, their immunoreactivity appears to reflect real melanopsin expression, rather than cross-reactivity of the antibody with an unrelated protein, because it disappears in melanopsin knockout animals (A. Castrucci and I. Provencio, personal communication; X. Qiu, J. Tong, and D. Berson, unpublished observations). The primate retina appears to contain two broadly similar subtypes of melanopsin-expressing ganglion cells, both of which are intrinsically photosensitive (Dacey et al., 2005).

If mouse M2 cells synthesize melanopsin protein, one should expect them to express β-galactosidase in the knock-in mice studied here. However, we have found no evidence for labeling of M2 cells in the retinas of these animals with either X-gal or the anti-β-galactosidase antibody. Dendrites that were stained well enough to trace invariably terminated in the outer IPL, like M1 but unlike M2 cells. Because the tau signal sequence was fused to the β-galactosidase protein, the marker enzyme was preferentially routed to axons, thus reducing its abundance and detectability in the somadendritic compartment. However, it seems very unlikely that labeling marked the axons but not the somata or dendrites of M2 cells because the number of labeled axons in the optic nerve closely matched the number of labeled somas (approximately 700 – 800). These counts, in turn, correspond well to estimates of the total number of M1 cells (A. Castrucci et al., unpublished observations). Thus, the most parsimonious interpretation appears to be that M2 cells do not express enough β-galactosidase to be detected by the methods used. This may be because the expression level of the melanopsin gene (and hence of the *tau-lacZ* marker gene) is lower in M2 than in M1 cells, as implied by the weaker melanopsin immunostaining in M2 than in M1 cells in wild-type animals (A. Castrucci et al., unpublished observations). Indeed, when anti-melanopsin immunostaining is suboptimal (e.g., by diluting primary antibody), only M1 cells are visible (unpublished observations). In summary, although some caution is warranted, the weight of the present evidence suggests that most if not all of the fiber labeling observed in the present study originates in M1 cells and thus from RGCs known to be directly photosensitive.

Suprachiasmatic nucleus

The present data confirm the well-established projection of photosensitive mRGCs to the SCN (Gooley et al. 2001, 2003; Berson et al., 2002; Hattar et al., 2002; Hannibal 2002, 2004; Berson, 2003; Sollars et al., 2003; Morin et al., 2004). The SCN has been subdivided into “core” and “shell” components on the basis of distinct patterns of chemoarchitecture and connections (Moore et al., 2002). The boundaries of these subregions are drawn differently by different investigators, in part because there is no consensus on how they should be defined (e.g.,

Abrahamson and Moore, 2001; Yan and Silver, 2002). The core has been reported to receive the bulk of the retinal input (Abrahamson and Moore, 2001; Moore et al., 2002) and, in turn, to relay photic information to the shell (Kriegsfeld et al., 2004), which may be the critical locus for light-induced circadian phase shifts (Yan and Silver, 2002). Our data weigh against this sort of serial model in the mouse, at least in its purest form, because they show that the axons of mRGCs terminate throughout the SCN as defined cytoarchitecturally or by the distribution of VIP-immunoreactive fibers, and certainly over a wider territory than the core as defined by Yan and Silver (2002). This evidence for substantial direct retinal innervation of the shell is in agreement with several earlier reports (Cassone et al. 1988; Castel et al., 1993) and suggests that the shell may not be exclusively dependent on the core for photic signals driving shifts in circadian phase.

The remarkable bilateral balance in input from mRGCs to the SCN parallels earlier observations on overall retinal input to the SCN in C57BL/6J mice (Abrahamson and Moore, 2001). Some bias in favor of crossed input has been reported in an albino strain of the house mouse (Miura et al., 1997) and in the white-footed mouse *Peromyscus leucopus* (Youngstrom and Nunez, 1986) This stands in marked contrast to the pronounced bias in favor of crossed projections observed in all other targets of mRGCs and suggests that most uncrossed mRGC axons end at the SCN and do not continue beyond it to the thalamus or brainstem.

Electrophysiological and behavioral evidence strongly suggests that conventional rod and cone photoreceptors can drive SCN unit responses and circadian phase shifts (Aggelopoulos and Meissl, 2000; Panda et al, 2002, 2003; Ruby et al., 2002; Lucas et al., 2003; Hattar et al, 2003). One possible route for such influences is through intraretinal synaptic inputs to mRGCs, which have been detected both ultrastructurally (Belenky et al., 2003) and electro-physiologically (Dunn and Berson, 2002; Dacey et al., 2005). However, an alternative pathway suggested by earlier retrograde tracing studies is a minor contribution of non-mRGCs to the retinohypothalamic tract (Gooley et al., 2003; Morin et al., 2003; Sollars et al., 2003; Hannibal and Fahrendrug, 2004). Although these earlier findings could arguably have been due to a failure to detect melanopsin protein or mRNA in some cells, the present data provide independent confirmation by showing that some β-galactosidase-negative (non-mRGC) axons innervate the SCN. Among the remaining challenges are to characterize the identity and functional properties of the non-mRGCs innervating the SCN; and to determine to what degree rod/cone influences reach the SCN directly from mRGCs, directly from non-mRGCs, or indirectly through polysynaptic circuits involving other brain nuclei.

Projections to other nuclei of the hypothalamus and limbic telencephalon

The mRGCs scatter a few afferent fibers through several preoptic nuclei. Among these is the VLPO, a key player in sleep regulation (Sherin et al., 1996), confirming earlier reports in the rat (Gooley et al., 2003; Hannibal and Fahrenkrug, 2004). Inputs from mRGCs to the preoptic region may provide a basis for photic modulation not only of sleep but also of circadian oscillations in core body temperature (Moore and Danchenko, 2002) or of neuroendocrine processes related to reproductive function. In agreement with the findings of Gooley et al. (2003) in the rat (but see Hannibal and Fahrenkrug, 2004) and of Morin et al. (2003) in the hamster, we find that retinal inputs to the vSPZ arise predominantly from mRGCs. This region, which also receives direct projections from the SCN, has been implicated in circadian and photic modulation of sleep and locomotor activity (Lu et al., 2001; Kramer et al., 2001; Moore and Danchenko, 2002).

The lateral hypothalamus, another destination of labeled axons in this study, is a well-known target of the retinohypothalamic tract. Leak and Moore (1997) suggested, on retinotopic grounds, that ganglion cells innervating the rat lateral hypothalamus differed from those projecting to the SCN. Our data, by contrast, indicate that in the mouse both of these projections

arise primarily from mRGCs. Another well-established target of the RHT is the supraoptic nucleus and/or the overlying adjacent peri-SON (e.g., Johnson et al., 1988; Levine et al., 1991, 1994; Mikkelsen and Serviere, 1992; Nakagawa et al., 1992; Ling et al., 1998; Abrahamson and Moore, 2001). This projection appears to influence the magnocellular neurons in the SON proper (Cui et al., 1997a,b) and may thus mediate photic modulation of neuroendocrine output. One possible reflection of such influence is the acute disruption by light of normal diurnal rhythms of plasma oxytocin and vasopressin (Windle et al., 1992; Kostoglou-Athanassiou et al., 1998). Our evidence indicates that some, although by no means all, of the direct retinal influence on the SON arises from intrinsically photosensitive RGCs.

Sparse retinal inputs to the medial amygdala have been reported previously (Johnson et al., 1988; Cooper et al.,. 1993; Elliott et al., 1995) and appear on the present evidence to arise in part from mRGCs. This region appears to be a site of integration of retinal input with signals from the olfactory system and IGL and may be one site where photic and olfactory stimuli converge to modulate reproductive behavior (Cooper, et al., 1994; Elliott et al., 1995; Morin and Blanchard, 1999).

Lateral geniculate complex

The present data confirm earlier reports that rodent mRGCs provide very little input to the LGd, the main thalamic relay of retinal information to the striate cortex (Hattar et al., 2002; Gooley et al.., 2004; Hannibal and Fahrenkrug, 2004). This suggests that, at least in rodents, mRGCs may exert little influence on visual perceptual mechanisms, consistent with the view that these RGCs form the foundation of a specialized non-image-forming visual network. However, a role for melanopsin RGCs in geniculocortical function should not be entirely excluded. We observed sparse fiber labeling in the LGd within a thin shell bounding the nucleus ventromedially and rostrally. The ventromedial region may correspond to the beta sector, a part of the murine LGd lying within the external medullary lamina (Godement, 1984), or to the alpha subdivision of the hamster LGd (Ling et al., 1997). The rostral zone may be related to the retinal input observed in the thalamic lateral posterior nucleus of some rodents (Ling et al., 1997). These thalamic targets are virtually certain to provide a conduit for signals from ganglion-cell photoreceptors to the visual cortex. In addition, mRGCs may influence cortical visual areas of the neocortex by less direct paths, because two of their brainstem targets, the olivary pretectal nucleus and superior colliculus, emit ascending projections to the visual thalamus. In monkeys, intrinsically photosensitive mRGCs have been reported to innervate the LGd directly on the basis of retrograde tracing evidence (Dacey et al., 2005), suggesting a possible role for mRGCs in cortical vision. However, humans with advanced outer retinal degeneration but preservation of non-image-forming visual responses presumably mediated by mRGCs (Provencio et al., 2000; Hannibal et al., 2004; Dacey et al., 2005) apparently lack any conscious appreciation of light (Czeisler et al. 1995; Klerman et al., 2002).

The IGL is clearly one of the major brain targets of mRGCs. Although it is a part of the geniculate complex, it does not project to the cortex but is, instead, a well-recognized component of the non-image-forming visual system. The IGL is reciprocally interconnected with the SCN and OPN, both of which are also targets of mRGCs, and has been implicated in circadian photoentrainment mechanisms (Harrington, 1997). Light responses of IGL neurons (Harrington and Rusak, 1989) are similar in several respects to those of mRGCs (Berson et al., 2002; Warren et al., 2003), including tonic ON responses that encode light intensity over a dynamic range of 2–3 log units.

The input from mRGCs to the IGL is much stronger from the contralateral than from the ipsilateral eye, as reported previously in the rodent for overall retinal input (Moore and Card, 1994; Muscat et al., 2003) and for mRGCs input in particular (Morin et al., 2003; Hannibal and Fahrenkrug, 2004). Ipsilateral-eye influence, which is predominantly inhibitory

(Harrington, 1997; Tang et al., 2002), appears to come not only by way of this direct pathway but also through an indirect pathway involving the contralateral IGL (Moore and Card, 1994; Harrington, 1997). Our data indicate that although the bulk of retinal afferents to the IGL arise from mRGCs, at least a small fraction of the input comes from non-mRGCs, in accord with observations in the hamster (Morin et al., 2003). Inputs from non-mRGCs are a possible source for OFF-center or transient light responses in the IGL (Harrington, 1997).

The boundaries of the IGL can be difficult to discern in conventional cell or fiber stains. It has been suggested that the nucleus be defined on the basis of its high concentration of neurons expressing neuropeptide Y (NPY) and its projections to the SCN and contralateral IGL (Morin et al., 1992; Morin and Blanchard, 1995; Harrington, 1997). The present results suggest that the presence of dense input from mRGCs may be a useful supplementary defining feature of the IGL. The nucleus is unmistakable in X-gal-stained coronal sections through the middle of the geniculate complex, bounded by regions where fiber labeling is virtually absent (the LGd) or relatively sparse (the LGv). This zone of dense fiber labeling extends forward from both its caudoventral and rostral poles into territory not traditionally included within the IGL. The caudoventral zone is traditionally included within the LGv (Harrington, 1997) but has been suggested to belong to the IGL in hamsters (Morin and Blanchard, 1995). The extension of the labeled terminal field from the rostral pole of the geniculate complex to the vicinity of the bed nucleus of the stria terminalis has been observed in several mammalian orders (Itaya et al., 1986; Johnson et al., 1988; Levine et al., 1991; Youngstrom et al., 1991; Cooper et al., 1993; Morin and Blanchard, 1995, 1999). The projection of mRGCs to this region was anticipated in a sense by the finding that this retinal terminal field is relatively hypertrophic in the blind mole rat, along with other relatively enlarged components of the non-image-forming visual nuclei (Cooper et al., 1993). Functional, connectional, and neurochemical studies will be needed to corroborate the provisional inclusion of these regions within the murine IGL.

As for the LGv, inputs from mRGCs clearly represent only a small fraction of its retinal afferents, in agreement with observations in the rat (Hannibal and Fahrenkrug, 2004). Few labeled fibers were present in the external division of the nucleus, which represents the major retinorecipient zone (Harrington, 1997). The densest labeling within the boundaries of the LGv as plotted by Paxinos and Franklin (2001) lies in two small regions that may well be part of the IGL, judging from the pattern of fiber labeling and its continuity with the IGL proper. The first, part of a possible rostral continuation of the IGL beyond the geniculate complex (see above), lies just ventrolateral to the rostral pole of the LGd. In hamsters, this region has been considered the anterior VLGNei by Harrington and colleagues (Harrington and Rusak, 1989; Harrington, 1997), but others have grouped it with the IGL on connectional and neurochemical grounds (Morin et al., 1992). The second, an apparent rostral extension of the caudoventral pole of the IGL, appears to occupy the caudal part of the internal division of the LGv.

Habenula and posterior limitans nucleus

The present findings demonstrate a substantial projection from mRGCs to a small zone lying at the dorsolateral margin of the lateral habenula. Retinal projections to this region were apparently first noted in the blind mole rat by Cooper et al. (1993) and in the rat by Qu et al. (1996) and have been observed subsequently in a variety of species (Morin and Blanchard, 1997; Reuss and Decker, 1997; Matteau et al., 2003). The functional role of the retinal projection to this region is not understood. Generally, the habenula is viewed as a relay from forebrain limbic centers and the striatum to the midbrain (Herkenham and Nauta, 1979). The lateral division of the lateral habenula, which lies closest to the retinal terminal zone, is implicated in polysynaptic pathways linking the entopeduncular nucleus (internal segment of globus pallidus) to the midbrain and pontine reticular formation (Kim and Chang, 2005). Light responses have been recorded throughout the habenula (Zhao et al., 2005), but these seem

unlikely to be driven by direct retinal input because most habenular cells appear to have dendritic arbors too restricted to reach the retinal terminal field (Kim and Chang, 2005). Indirect pathways may instead be responsible (Zhao et al., 2005). In the cod, a teleost fish, melanopsin is expressed in cells within the lateral part of the habenula (Drivenes et al., 2003), and similar observations have been made in the chick (Chaurasia et al., 2005). The habenula is embryologically associated with the pineal and appears to be connected to it synaptically (e.g., Ronnekliev et al., 1980; Ronnekliev and Kelly, 1984; Moller and Baeres, 2002). The mammalian pineal appears to be strongly influenced by mRGCs, but this influence has been thought to be very indirect, routed through a polysynaptic circuit including the SCN and sympathetic nervous system (for review, see Berson, 2003). There was nothing in our material to suggest the presence of melanopsin-expressing cells or mRGC axons in the pineal or its stalk.

In hamster, Morin and Blanchard (1997) consider the peri-habenular retinorecipient terminal field to be a rostral continuation of the posterior limitans nucleus, which they view as a component of what they have termed the subcortical visual shell (Morin and Blanchard, 1998). This shell, comprising a constellation of functionally and connectionally interrelated retinorecipient nuclei, includes the SCN, OPN, and IGL, all of which are targets of mRGCs. The main body of the posterior limitans nucleus lies just lateral to the anterior pretectal nucleus, where it abuts the dorsal thalamus. In rats, mRGCs have been inferred to project to this region (Hannibal and Fahrenkrug, 2004; see also Pritchard et al., 2002), but a comparable pathway appears to be very weak in the mouse, judging from our material.

OPN and other pretectal nuclei

Dense terminations of β-galactosidase-labeled fibers demarcate a small portion of the retinorecipient pretectum. This field corresponds largely to the olivary pretectal nucleus as described in atlases and experimental studies in rodents (Scalia, 1972; Scalia and Arango, 1979; Mikkelsen, 1992; Morin and Blanchard, 1997; Paxinos and Franklin, 2001). The OPN is a critical element in the pathway mediating the pupillary light reflex (Trejo and Cicerone, 1984; Clarke and Ikeda, 1985; Young and Lund, 1994), and the role of mRGCs in pupillary function is well established (Lucas et al., 2001, 2003; Hattar et al, 2002, 2003; Panda et al., 2003). Neurons in the OPN have tonic, irradiance-encoding light responses that resemble those of the intrinsically photosensitive ganglion cells that innervate them (Trejo and Cicerone, 1984; Clarke and Ikeda, 1985). However, our data indicate that the OPN receives convergent input from non-mRGCs as well, as inferred for other rodents on the basis of retrograde tracing data (Gooley et al., 2003; Morin et al., 2003). Both mRGCs and non-mRGCs are thus potential sources of the rod and/or cone signals known to reach the pupillomotor centers (Lucas et al., 2001; Hattar et al., 2003).

The OPN has been difficult to define in most prior studies because it is indistinct in conventional cell and fiber stains and even in retinofugal fiber labeling studies, due to its contiguity with other retinorecipient nuclei. The specificity of mRGC input suggests that this may be one useful defining characteristic of the nucleus. Other potentially specific markers for the OPN include parvalbumin immunoreactivity, induction of the immediate early gene c-fos by light, and selective labeling by axonally transported adenoassociated virus injected into the eye (Okoyama and Moriizumi, 2001; Prichard et al., 2002; Gooley et al., 2004). All three of these markers, like the X-gal staining, reveal the hollow ovoid form of the rostral portion of the nucleus as viewed in coronal sections. Further study correlating these various markers would help to define the boundaries of this nucleus. On present evidence, though, the OPN would appear to extend farther caudally and laterally than commonly recognized, invading territory often included in the posterior pretectal nucleus and nucleus of the optic tract and terminating just below the dorsal terminal nucleus of the accessory optic system.

The OPN may have functional roles beyond pupillary control. For example, there are substantial ascending projections from the OPN to the SCN, IGL, LGv, and lateral posterior-pulvinar complex of the thalamus (Weber et al., 1986; Mikkelsen and Vrang, 1994; Klooster et al., 1995; Moga and Moore, 1997; Morin and Blanchard, 1998). The retinal projection to the OPN is robust in the blind mole rat, despite the absence of any iris or ciliary body in its eye (Cooper et al., 1993).

Few mRGC axons extend beyond the confines of the OPN, as we have defined it, to other pretectal nuclei. The most prominent target of such fibers is a region of the deep pretectum in and around the nucleus of the posterior commissure. This area exhibits light-dependent induction of immediate early genes, as do many of the other targets of mRGCs (Prichard et al., 2002). Some fibers continue beyond this region to reach the rostral periaqueductal gray, a region that also receives input from the OPN and projects to autonomic pupillary control centers (Klooster et al., 1995; Klooster and Vrensen, 1998). In some mammalian species, fibers continue along this trajectory to innervate the dorsal raphe nucleus (Fite et al., 1999). However, in mouse this pathway is extremely weak, and except for a single fiber in one animal, we have not seen β-galactosidase-positive fibers in this nucleus.

Superior colliculus

Our data demonstrate an unequivocal, if relatively sparse, projection from mRGCs to the murine superior colliculus. Similar findings were reported by Morin et al. (2003) in the hamster. In the rat, several indirect lines of evidence suggest a possible sparse collicular innervation by the axons of mRGCs (Gooley et al., 2003; Hannibal and Fahrenkrug, 2004), but Gooley et al. (2003) were unable to label mRGCs by retrograde transport from the SC. Our data show that mRGC afferents terminate throughout the full thickness of the superficial, retinorecipient collicular laminae (Frost et al., 1986). The morphology of these afferents did not match that of either of the two types of retinotectal arbors so far described in mouse (Frost et al., 1986), presumably because they are a tiny minority of retinotectal afferents and would have been unlikely to appear in a random sample of such fibers.

Although they are present throughout the collicular map, terminations of mRGC axons are heaviest in the medial third of the colliculus (Fig. 10A), representing the upper visual field (Drager and Hubel, 1976). If mRGCs adhere to the retinotopic ordering characteristic of the retinocollicular projection, this would indicate a particularly heavy projection from mRGCs in the inferior retina. This seems to be at odds with reports indicating somewhat higher mRGC density in the superior than in the inferior retina (Hannibal et al., 2002;Hattar et al., 2002; but see Morin et al., 2003 and Sollars et al., 2003). However, the assumption of conventional topographic order may be unwarranted. Whereas the overall uncrossed retinotectal projection is concentrated in a small collicular zone representing the binocular visual field (Godement et al., 1984), the uncrossed input from mRGCs is far more widespread. It clearly encroaches on the representation of the contralateral temporal visual field, which cannot be seen by the eye from which these retinofugal fibers arise. At least one target of melanopsin RGCs, the IGL, lacks obvious retinotopic order (Harrington, 1997), and it may be that this unique ganglion cell population spurns retinotopy even when projecting to highly retinotopic targets. Neurons in the superficial collicular layers contribute to orienting movements toward visual targets by virtue of their descending influence on the deeper collicular layers (Isa, 2002). They may also participate in cortical visual mechanisms through ascending projections to thalamic visual nuclei. Both of these functions call for considerable spatial fidelity, so a lack of retinotopy in the mRGC input may suggest that these ganglion cells play a modulatory role in the colliculus, rather than conveying information about target location or identity (see, e.g., Barash et al., 1998).

Acknowledgments

We thank Motoharu Takao for technical help on the cholera toxin experiments, Mary Blue and Jonathan Bradley for assistance with histology and interpretation of labeling distributions, Valerie Maine for technical help, and Yuqin Liang for assistance with genotyping.

Grant sponsor: the National Eye Institute; Grant number: 5R01 EY014596 (to K.-W.Y.); Grant number: 5 R01 EY012793 (to D.B.).

Abbreviations

AH	anterior hypothalamic nucleus
AHP	anterior hypothalamic area, posterior
AP	anterior pretectal nucleus
AV	anteroventral thalamic nucleus
BST	bed nucleus of the stria terminalis
CL	central lateral thalamic nucleus
CP	cerebral peduncle
f	fornix
fr	fasciculus retroflexus
hc	habenular commissure
ic	internal capsule
IGL	intergeniculate leaflet
LD	lateral dorsal thalamic nucleus
LGd	lateral geniculate nucleus, dorsal division
LGv	lateral geniculate nucleus, ventral division
LH	lateral hypothalamus
LHb	lateral habenula
LP	lateral posterior thalamic nucleus
LPO	lateral preoptic area
MA	medial amygdaloid nucleus
MHb	medial habenula
MPO	medial preoptic area
OPN	olivary pretectal nucleus
ot	optic tract
ox	optic chiasm
PAG	periaqueductal gray
pc	posterior commissure
PO	preoptic area
pSON	peri-supraoptic nucleus
SC	superior colliculus

SCN	suprachiasmatic nucleus
SGS	stratum griseum superficiale of the superior colliculus
SI	substantia innominata
sm	stria medullaris
SO	stratum opticum of the superior colliculus
st	stria terminalis
SPZ	subparaventricular zone
SZ	stratum zonale of the superior colliculus
st	stria terminalis
VLPO	ventrolateral preoptic area
VMH	ventromedial hypothalamus
vSPZ	ventral subparaventricular zone

LITERATURE CITED

Abrahamson EE, Moore RY. Suprachiasmatic nucleus in the mouse: retinal innervation, intrinsic organization and efferent projections. Brain Res 2001;916:172–191. [PubMed: 11597605]

Aggelopoulos NC, Meissl H. Responses of neurones of the rat suprachiasmatic nucleus to retinal illumination under photopic and scotopic conditions. J Physiol (Lond) 2000;523:211–222. [PubMed: 10673556]

Alvarez-Lopez C, Cernuda-Cernuda R, Paniagua MA, Alvarez-Viejo M, Fernandez-Lopez A, Garcia-Fernandez JM. The transcription factor CREB is phosphorylated in neurons of the piriform cortex of blind mice in response to illumination of the retina. Neurosci Lett 2004;357:223–226. [PubMed: 15003290]

Barash S, Melikyan A, Sivakov A, Tauber M. Shift of visual fixation dependent on background illumination. J Neurophysiol 1998;79:2766–2781. [PubMed: 9582243]

Belenky MA, Smeraski CA, Provencio I, Sollars PJ, Pickard GE. Melanopsin retinal ganglion cells receive bipolar and amacrine cell synapses. J Comp Neurol 2003;460:380–393. [PubMed: 12692856]

Berson DM. Strange vision: ganglion cells as circadian photoreceptors. Trends Neurosci 2003;26:314–320. [PubMed: 12798601]

Berson DM, Dunn FA, Takao M. Phototransduction by retinal ganglion cells that set the circadian clock. Science 2002;295:1070–1073. [PubMed: 11834835]

Cassone VM, Speh JC, Card JP, Moore RY. Comparative anatomy of the mammalian hypothalamic suprachiasmatic nucleus. J Biol Rhythms 1988;3:71–91. [PubMed: 2979633]

Castel M, Belenky M, Cohen S, Ottersen OP, Storm-Mathisen J. Glutamate-like immunoreactivity in retinal terminals of the mouse suprachiasmatic nucleus. Eur J Neurosci 1993;5:368–381. [PubMed: 7903187]

Chaurasia SS, Rollag MD, Jiang G, Hayes WP, Haque R, Natesan A, Zatz M, Tosini G, Liu C, Korf HW, Iuvone PM, Provencio I. Molecular cloning, localization and circadian expression of chicken melanopsin (Opn4): differential regulation of expression in pineal and retinal cell types. J Neurochem 2005;92:158–170. [PubMed: 15606905]

Clarke RJ, Ikeda H. Luminance and darkness detectors in the olivary and posterior pretectal nuclei and their relationship to the pupillary light reflex in the rat. I. Studies with steady luminance levels. Exp Brain Res 1985;57:224–232. [PubMed: 3972027]

Cooper HM, Herbin M, Nevo E. Visual system of a naturally microphthalmic mammal: the blind mole rat, *Spalax ehrenbergi*. J Comp Neurol 1993;328:313–350. [PubMed: 8440785]

Cooper HM, Parvopassu F, Herbin M, Magnin M. Neuroanatomical pathways linking vision and olfaction in mammals. Psychoneuroendocrinology 1994;19:623–639. [PubMed: 7938360]

Cui LN, Jolley CJ, Dyball RE. Electrophysiological evidence for retinal projections to the hypothalamic supraoptic nucleus and its perinuclear zone. J Neuroendocrinol 1997a;9:347–353. [PubMed: 9181488]

Cui LN, Saeb-Parsy K, Dyball RE. Neurones in the supraoptic nucleus of the rat are regulated by a projection from the suprachiasmatic nucleus. J Physiol 1997b;502:149–159. [PubMed: 9234203]

Czeisler CA, Shanahan TL, Klerman EB, Martens H, Brotman DJ, Emens JS, Klein T, Rizzo JFd. Suppression of melatonin secretion in some blind patients by exposure to bright light [see comments]. N Engl J Med 1995;332:6–11. [PubMed: 7990870]

Dacey DM, Liao HW, Peterson BB, Robinson FR, Smith VC, Pokorny J, Yau KW, Gamlin PD. Melanopsin-expressing ganglion cells in primate retina signal colour and irradiance and project to the LGN. Nature 2005;433:749–754. [PubMed: 15716953]

Drager UC, Hubel DH. Topography of visual and somatosensory projections to mouse superior colliculus. J Neurophysiol 1976;39:91–101. [PubMed: 1249606]

Drager UC, Olsen JF. Origins of crossed and uncrossed retinal projections in pigmented and albino mice. J Comp Neurol 1980;191:383–412. [PubMed: 7410600]

Drivenes O, Soviknes AM, Ebbesson LO, Fjose A, Seo HC, Helvik JV. Isolation and characterization of two teleost melanopsin genes and their differential expression within the inner retina and brain. J Comp Neurol 2003;456:84–93. [PubMed: 12508316]

Dunn FA, Berson DM. Are intrinsically photosensitive retinal ganglion cells influenced by rods or cones? Abstract #2982, Association for Research in Vision and Ophthalmology, Ft. Lauderdale, FL; May 2002;8:2002.

Elliott AS, Weiss ML, Nunez AA. Direct retinal communication with the peri-amygdaloid area. Neuroreport 1995;6:806–808. [PubMed: 7541657]

Fite KV, Janusonis S, Foote W, Bengston L. Retinal afferents to the dorsal raphe nucleus in rats and Mongolian gerbils. J Comp Neurol 1999;414:469–484. [PubMed: 10531540]

Frost DO, Edwards MA, Sachs GM, Caviness VS Jr. Retinotectal projection in reeler mutant mice: relationships among axon trajectories, arborization patterns and cytoarchitecture. Brain Res 1986;393:109–120. [PubMed: 3730887]

Fu Y, Zhong H, Wang MH, Luo D-G, Liao H-W, Maeda H, Hattar S, Frishman LJ, Yau K-W. Intrinsically photosensitive retinal ganglion cells detect light with a vitamin A-based photopigment, melanopsin. Proc Natl Acad Sci U S A 2005;102:10339–10344. [PubMed: 16014418]

Godement P, Salaun J, Imbert M. Prenatal and postnatal development of retinogeniculate and retinocollicular projections in the mouse. J Comp Neurol 1984;230:552–575. [PubMed: 6520251]

Gooley JJ, Lu J, Chou TC, Scammell TE, Saper CB. Melanopsin in cells of origin of the retinohypothalamic tract. Nat Neurosci 2001;4:1165. [PubMed: 11713469]

Gooley JJ, Lu J, Fischer D, Saper CB. A broad role for melanopsin in nonvisual photoreception. J Neurosci 2003;23:7093–7106. [PubMed: 12904470]

Hannibal J, Fahrenkrug J. Target areas innervated by PACAP-immunoreactive retinal ganglion cells. Cell Tissue Res 2004;316:99–113. [PubMed: 14991397]

Hannibal J, Hindersson P, Knudsen SM, Georg B, Fahrenkrug J. The photopigment melanopsin is exclusively present in pituitary adenylate cyclase-activating polypeptide-containing retinal ganglion cells of the retinohypothalamic tract. J Neurosci 2002;22:RC191. [PubMed: 11756521]

Hannibal J, Hindersson P, Ostergaard J, Georg B, Heegaard S, Larsen PJ, Fahrenkrug J. Melanopsin is expressed in PACAP-containing retinal ganglion cells of the human retinohypothalamic tract. Invest Ophthalmol Vis Sci 2004;45:4202–4209. [PubMed: 15505076]

Harrington ME. The ventral lateral geniculate nucleus and the intergeniculate leaflet: interrelated structures in the visual and circadian systems. Neurosci Biobehav Rev 1997;21:705–727. [PubMed: 9353800]

Harrington ME, Rusak B. Photic responses of geniculo-hypothalamic tract neurons in the Syrian hamster. Vis Neurosci 1989;2:367–375. [PubMed: 2487659]

Hattar S, Liao HW, Takao M, Berson DM, Yau KW. Melanopsin-containing retinal ganglion cells: architecture, projections, and intrinsic photosensitivity. Science 2002;295:1065–1070. [PubMed: 11834834]

Hattar S, Lucas RJ, Mrosovsky N, Thompson S, Douglas RH, Hankins MW, Lem J, Biel M, Hofmann F, Foster RG, Yau KW. Melanopsin and rod-cone photoreceptive systems account for all major accessory visual functions in mice. Nature 2003;424:76–81. [PubMed: 12808468]

Herkenham M, Nauta WJ. Efferent connections of the habenular nuclei in the rat. J Comp Neurol 1979;187:19–47. [PubMed: 226566]

Hirota T, Fukada Y. Resetting mechanism of central and peripheral circadian clocks in mammals. Zool Sci 2004;21:359–368. [PubMed: 15118222]

Isa T. Intrinsic processing in the mammalian superior colliculus. Curr Opin Neurobiol 2002;12:668–677. [PubMed: 12490257]

Itaya SK, Van Hoesen GW, Benevento LA. Direct retinal pathways to the limbic thalamus of the monkey. Exp Brain Res 1986;61:607–613. [PubMed: 3754221]

Johnson RF, Morin LP, Moore RY. Retinohypothalamic projections in the hamster and rat demonstrated using cholera toxin. Brain Res 1988;462:301–312. [PubMed: 3191391]

Kim U, Chang SY. Dendritic morphology, local circuitry, and intrinsic electrophysiology of neurons in the rat medial and lateral habenular nuclei of the epithalamus. J Comp Neurol 2005;483:236–250. [PubMed: 15678472]

Klerman EB, Shanahan TL, Brotman DJ, Rimmer DW, Emens JS, Rizzo JF 3rd, Czeisler CA. Photic resetting of the human circadian pacemaker in the absence of conscious vision. J Biol Rhythms 2002;17:548–555. [PubMed: 12465888]

Klooster J, Vrensen GF. New indirect pathways subserving the pupillary light reflex: projections of the accessory oculomotor nuclei and the periaqueductal gray to the Edinger-Westphal nucleus and the thoracic spinal cord in rats. Anat Embryol (Berl) 1998;198:123–132. [PubMed: 9725771]

Klooster J, Vrensen GF, Muller LJ, van der Want JJ. Efferent projections of the olivary pretectal nucleus in the albino rat subserving the pupillary light reflex and related reflexes. A light microscopic tracing study. Brain Res 1995;688:34–46. [PubMed: 8542320]

Kostoglou-Athanassiou I, Treacher DF, Wheeler MJ, Forsling ML. Bright light exposure and pituitary hormone secretion. Clin Endocrinol (Oxf) 1998;48:73–79. [PubMed: 9509071]

Kramer A, Yang FC, Snodgrass P, Li X, Scammell TE, Davis FC, Weitz CJ. Regulation of daily locomotor activity and sleep by hypothalamic EGF receptor signaling. Science 2001;294:2511–2515. [PubMed: 11752569]

Kriegsfeld LJ, Leak RK, Yackulic CB, LeSauter J, Silver R. Organization of suprachiasmatic nucleus projections in Syrian hamsters (*Mesocricetus auratus*): an anterograde and retrograde analysis. J Comp Neurol 2004;468:361–379. [PubMed: 14681931]

Leak RK, Moore RY. Identification of retinal ganglion cells projecting to the lateral hypothalamic area of the rat. Brain Res 1997;770:105–114. [PubMed: 9372209]

Levine JD, Weiss ML, Rosenwasser AM, Miselis RR. Retinohypothalamic tract in the female albino rat: a study using horseradish peroxidase conjugated to cholera toxin. J Comp Neurol 1991;306:344–360. [PubMed: 1711060]

Levine JD, Zhao XS, Miselis RR. Direct and indirect retinohypothalamic projections to the supraoptic nucleus in the female albino rat. J Comp Neurol 1994;341:214–224. [PubMed: 8163725]

Ling C, Schneider GE, Northmore D, Jhaveri S. Afferents from the colliculus, cortex, and retina have distinct terminal morphologies in the lateral posterior thalamic nucleus. J Comp Neurol 1997;388:467–483. [PubMed: 9368854]

Ling C, Schneider GE, Jhaveri S. Target-specific morphology of retinal axon arbors in the adult hamster. Vis Neurosci 1998;15:559–579. [PubMed: 9685208]

Lu J, Zhang YH, Chou TC, Gaus SE, Elmquist JK, Shiromani P, Saper CB. Contrasting effects of ibotenate lesions of the paraventricular nucleus and subparaventricular zone on sleep-wake cycle and temperature regulation. J Neurosci 2001;21:4864–4874. [PubMed: 11425913]

Lucas RJ, Douglas RH, Foster RG. Characterization of an ocular photopigment capable of driving pupillary constriction in mice. Nat Neurosci 2001;4:621–626. [PubMed: 11369943]

Lucas RJ, Hattar S, Takao M, Berson DM, Foster RG, Yau K-W. Diminished pupillary light reflex at high irradiances in melanopsin-knockout mice. Science 2003;299:245–247. [PubMed: 12522249]

Matteau I, Boire D, Ptito M. Retinal projections in the cat: a cholera toxin B subunit study. Vis Neurosci 2003;20:481–493. [PubMed: 14977327]

Melyan Z, Tarttelin EE, Bellingham J, Lucas RJ, Hankins MW. Addition of human melanopsin renders mammalian cells photoresponsive. Nature 2005;433:741–745. [PubMed: 15674244]

Mick G, Cooper H, Magnin M. Retinal projection to the olfactory tubercle and basal telencephalon in primates. J Comp Neurol 1993;327:205–219. [PubMed: 8425942]

Mikkelsen JD. Visualization of efferent retinal projections by immunohistochemical identification of cholera toxin subunit B. Brain Res Bull 1992;28:619–623. [PubMed: 1617444]

Mikkelsen JD, Serviere J. Demonstration of a direct projection from the retina to the hypothalamic supraoptic nucleus of the hamster. Neurosci Lett 1992;139:149–152. [PubMed: 1376875]

Mikkelsen JD, Vrang N. A direct pretectosuprachiasmatic projection in the rat. Neuroscience 1994;62:497–505. [PubMed: 7530345]

Miura M, Dong K, Ahmed FA, Okamura H, Yamadori T. The termination of optic nerve fibers in the albino mouse. Kobe J Med Sci 1997;43:99–108. [PubMed: 9489295]

Moga MM, Moore RY. Organization of neural inputs to the suprachiasmatic nucleus in the rat. J Comp Neurol 1997;389:508–534. [PubMed: 9414010]

Moller M, Baeres FM. The anatomy and innervation of the mammalian pineal gland. Cell Tissue Res 2002;309:139–150. [PubMed: 12111544]

Mombaerts P, Wang F, Dulac C, Chao SK, Nemes A, Mendelsohn M, Edmondson J, Axel R. Visualizing an olfactory sensory map. Cell 1996;87:675–686. [PubMed: 8929536]

Moore RY, Card JP. Intergeniculate leaflet: an anatomically and functionally distinct subdivision of the lateral geniculate complex. J Comp Neurol 1994;344:403–430. [PubMed: 8063960]

Moore RY, Danchenko RL. Paraventricular-subparaventricular hypothalamic lesions selectively affect circadian function. Chronobiol Int 2002;19:345–360. [PubMed: 12025929]

Moore RY, Speh JC, Leak RK. Suprachiasmatic nucleus organization. Cell Tissue Res 2002;309:89–98. [PubMed: 12111539]

Morin LP, Blanchard J. Organization of the hamster intergeniculate leaflet: NPY and ENK projections to the suprachiasmatic nucleus, intergeniculate leaflet and posterior limitans nucleus. Vis Neurosci 1995;12:57–67. [PubMed: 7536441]

Morin LP, Blanchard JH. Neuropeptide Y and enkephalin immunoreactivity in retinorecipient nuclei of the hamster pretectum and thalamus. Vis Neurosci 1997;14:765–777. [PubMed: 9279004]

Morin LP, Blanchard JH. Interconnections among nuclei of the subcortical visual shell: the intergeniculate leaflet is a major constituent of the hamster subcortical visual system. J Comp Neurol 1998;396:288–309. [PubMed: 9624585]

Morin LP, Blanchard JH. Forebrain connections of the hamster intergeniculate leaflet: comparison with those of ventral lateral geniculate nucleus and retina. Vis Neurosci 1999;16:1037–1054. [PubMed: 10614586]

Morin LP, Blanchard J, Moore RY. Intergeniculate leaflet and suprachiasmatic nucleus organization and connections in the golden hamster. Vis Neurosci 1992;8:219–230. [PubMed: 1372173]

Morin LP, Blanchard JH, Provencio I. Retinal ganglion cell projections to the hamster suprachiasmatic nucleus, intergeniculate leaflet, and visual midbrain: bifurcation and melanopsin immunoreactivity. J Comp Neurol 2003;465:401–416. [PubMed: 12966564]

Mrosovsky N, Hattar S. Impaired masking responses to light in melanopsin-knockout mice. Chronobiol Int 2003;20:989–999. [PubMed: 14680139]

Muscat L, Huberman AD, Jordan CL, Morin LP. Crossed and uncrossed retinal projections to the hamster circadian system. J Comp Neurol 2003;466:513–524. [PubMed: 14566946]

Nakagawa S, Tamai Y, Yasui M, Konishi N. Termination of retinal fibers in lateral preoptic and hypothalamic areas of the crab-eating monkey, Macaca irus. Arch Histol Jpn 1982;45:207–212. [PubMed: 7125863]

Newman LA, Walker MT, Brown RL, Cronin TW, Robinson PR. Melanopsin forms a functional short-wavelength photopigment. Biochemistry 2003;42:12734–12738. [PubMed: 14596587]

Okoyama S, Moriizumi T. Onset of calbindin-D 28K and parvalbumin expression in the lateral geniculate complex and olivary pretectal nucleus during postnatal development of the rat. Int J Dev Neurosci 2001;19:655–661. [PubMed: 11705670]

Pak MW, Giolli RA, Pinto LH, Mangini NJ, Gregory KM, Vanable JW Jr. Retinopretectal and accessory optic projections of normal mice and the OKN-defective mutant mice beige, beige-J, and pearl. J Comp Neurol 1987;258:435–446. [PubMed: 3584547]

Panda S, Sato TK, Castrucci AM, Rollag MD, DeGrip WJ, Hogenesch JB, Provencio I, Kay SA. Melanopsin (Opn4) requirement for normal light-induced circadian phase shifting. Science 2002;298:2213–2216. [PubMed: 12481141]

Panda S, Provencio I, Tu DC, Pires SS, Rollag MD, Castrucci AM, Pletcher MT, Sato TK, Wiltshire T, Andahazy M, Kay SA, Van Gelder RN, Hogenesch JB. Melanopsin is required for non-image-forming photic responses in blind mice. Science 2003;301:525–527. [PubMed: 12829787]

Panda S, Nayak SK, Campo B, Walker JR, Hogenesch JB, Jegla T. Illumination of the melanopsin signaling pathway. Science 2005;307:600–604. [PubMed: 15681390]

Paxinos, G.; Franklin, KBJ. The mouse brain in stereotaxic coordinates. San Diego: Academic Press; 2001.

Pickard GE, Silverman AJ. Direct retinal projections to the hypothalamus, piriform cortex, and accessory optic nuclei in the golden hamster as demonstrated by a sensitive anterograde horseradish peroxidase technique. J Comp Neurol 1981;196:155–172. [PubMed: 7204664]

Prichard JR, Stoffel RT, Quimby DL, Obermeyer WH, Benca RM, Behan M. Fos immunoreactivity in rat subcortical visual shell in response to illuminance changes. Neuroscience 2002;114:781–793. [PubMed: 12220578]

Provencio I, Jiang G, De Grip WJ, Hayes WP, Rollag MD. Melanopsin: an opsin in melanophores, brain, and eye. Proc Natl Acad Sci U S A 1998;95:340–345. [PubMed: 9419377]

Provencio I, Rodriguez IR, Jiang G, Hayes WP, Moreira EF, Rollag MD. A novel human opsin in the inner retina. J Neurosci 2000;20:600–605. [PubMed: 10632589]

Provencio I, Rollag MD, Castrucci AM. Photoreceptive net in the mammalian retina. Nature 2002;415:493. [PubMed: 11823848]

Qiu X, Kumbalasiri T, Carlson SM, Wong KY, Krishna V, Provencio I, Berson DM. Induction of photosensitivity by heterologous expression of melanopsin. Nature 2005;433:745–749. [PubMed: 15674243]

Qu T, Dong K, Sugioka K, Yamadori T. Demonstration of direct input from the retina to the lateral habenular nucleus in the albino rat. Brain Res 1996;709:251–258. [PubMed: 8833761]

Reuss S, Decker K. Anterograde tracing of retinohypothalamic afferents with Fluoro-Gold. Brain Res 1997;745:197–204. [PubMed: 9037410]

Ronnekleiv OK, Kelly MJ. Distribution of substance P neurons in the epithalamus of the rat: an immunohistochemical investigation. J Pineal Res 1984;1:355–370. [PubMed: 6085878]

Ronnekleiv OK, Kelly MJ, Wuttke W. Single unit recordings in the rat pineal gland: evidence for habenulo–pineal neural connections. Exp Brain Res 1980;39:187–192. [PubMed: 7398816]

Ruby NF, Brennan TJ, Xie X, Cao V, Franken P, Heller HC, O'Hara BF. Role of melanopsin in circadian responses to light. Science 2002;298:2211–2213. [PubMed: 12481140]

Scalia F. The termination of retinal axons in the pretectal region of mammals. J Comp Neurol 1972;145:223–257. [PubMed: 4555428]

Scalia F, Arango V. Topographic organization of the projections of the retina to the pretectal region in the rat. J Comp Neurol 1979;186:271–292. [PubMed: 447885]

Sherin JE, Shiromani PJ, McCarley RW, Saper CB. Activation of ventrolateral preoptic neurons during sleep. Science 1996;271:216–219. [PubMed: 8539624]

Sollars PJ, Smeraski CA, Kaufman JD, Ogilvie MD, Provencio I, Pickard GE. Melanopsin and non-melanopsin expressing retinal ganglion cells innervate the hypothalamic suprachiasmatic nucleus. Vis Neurosci 2003;20:601–610. [PubMed: 15088713]

Tang IH, Murakami DM, Fuller CA. Unilateral optic nerve transection alters light response of suprachiasmatic nucleus and intergeniculate leaflet. Am J Physiol Regul Integr Comp Physiol 2002;282:R569–577. [PubMed: 11792668]

Trejo LJ, Cicerone CM. Cells in the pretectal olivary nucleus are in the pathway for the direct light reflex of the pupil in the rat. Brain Res 1984;300:49–62. [PubMed: 6733467]

Warren EJ, Allen CN, Brown RL, Robinson DW. Intrinsic light responses of retinal ganglion cells projecting to the circadian system. Eur J Neurosci 2003;17:1727–1735. [PubMed: 12752771]

Weber JT, Chen IL, Hutchins B. The pretectal complex of the cat: cells of origin of projections to the pulvinar nucleus. Brain Res 1986;397:389–394. [PubMed: 3801879]

Windle RJ, Forsling ML, Guzek JW. Daily rhythms in the hormone content of the neurohypophysial system and release of oxytocin and vasopressin in the male rat: effect of constant light. J Endocrinol 1992;133:283–290. [PubMed: 1613430]

Yan L, Silver R. Differential induction and localization of mPer1 and mPer2 during advancing and delaying phase shifts. Eur J Neurosci 2002;16:1531–1540. [PubMed: 12405967]

Yoshimura T, Ebihara S. Spectral sensitivity of photoreceptors mediating phase-shifts of circadian rhythms in retinally degenerate CBA/J (rd/rd) and normal CBA/N (+/+)mice. J Comp Physiol [A] 1996;178:797–802.

Young MJ, Lund RD. The anatomical substrates subserving the pupillary light reflex in rats: origin of the consensual pupillary response. Neuroscience 1994;62:481–496. [PubMed: 7830893]

Youngstrom TG, Nunez AA. Comparative anatomy of the retinohypothalamic tract in photoperiodic and non-photoperiodic rodents. Brain Res Bull 1986;17:485–492. [PubMed: 2430681]

Youngstrom TG, Weiss ML, Nunez AA. Retinofugal projections to the hypothalamus, anterior thalamus and basal forebrain in hamsters. Brain Res Bull 1991;26:403–411. [PubMed: 2049607]

Zhao H, Rusak B. Circadian firing-rate rhythms and light responses of rat habenular nucleus neurons in vivo and in vitro. Neuroscience 2005;132:519–528. [PubMed: 15802202]

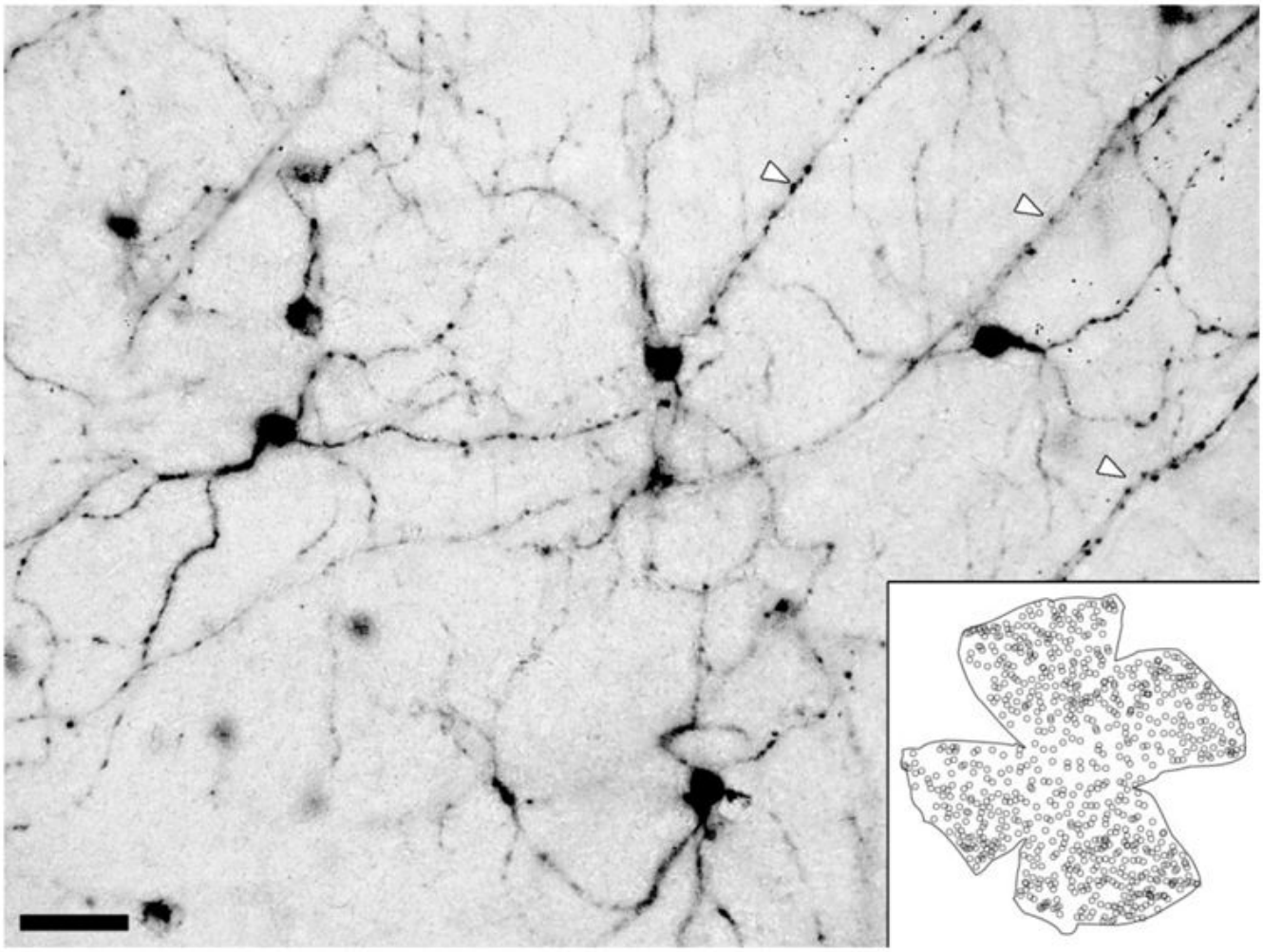

Fig. 1.

X-gal labeling of melanopsin ganglion cells in a retinal wholemount. Composite image derived from a stack of brightfield photomicrographs locally masked to reveal all labeled processes in sharp focus. Arrowheads mark axons in the optic fiber layer. **Inset:** Schematic charting of distribution of X-gal-labeled cell bodies in one retinal wholemount. Scale bar = 50 μm.

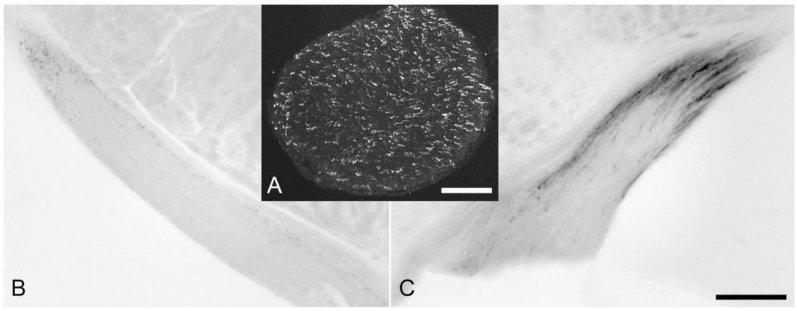

Fig. 2.

Distribution of axons of mRGCs in optic nerve and tract. **A:** Confocal image of axonal anti-β-galactosidase immunoreactivity in a transverse section of the optic nerve. **B,C:** X-gal staining of axons in the optic tract contralateral (B) and ipsilateral (C) to a monocular enucleation. Axonal degeneration is almost complete in B but nearly absent in C, indicating that, beyond the SCN, melanopsin RGCs have predominantly crossed projections. Scale bar = 100 μm in A; 200 μm in C (applies to B,C).

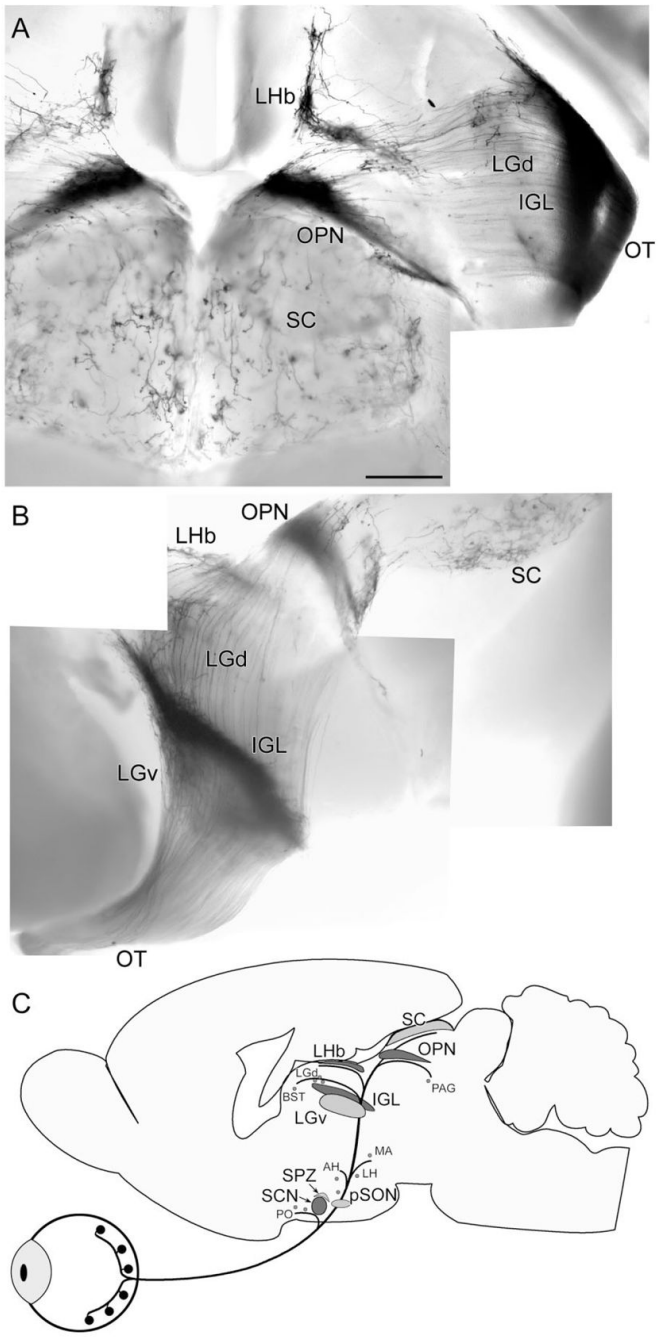

Fig. 3.

Overview of axonal projections of mRGCs. A,B: Whole brains stained by X-gal. **A:** Dorsal view, with rostral at the top. **B:** Lateral view with rostral at the left and dorsal at the top. **C:** Schematic drawing illustrating nuclear targets of melanopsin RGCs. Principle targets are shown in dark gray and secondary targets in light gray. Minor targets are indicated by small lettering and dots. For abbreviations, see list. Scale bar = 500 μm in A (applies to A,B).

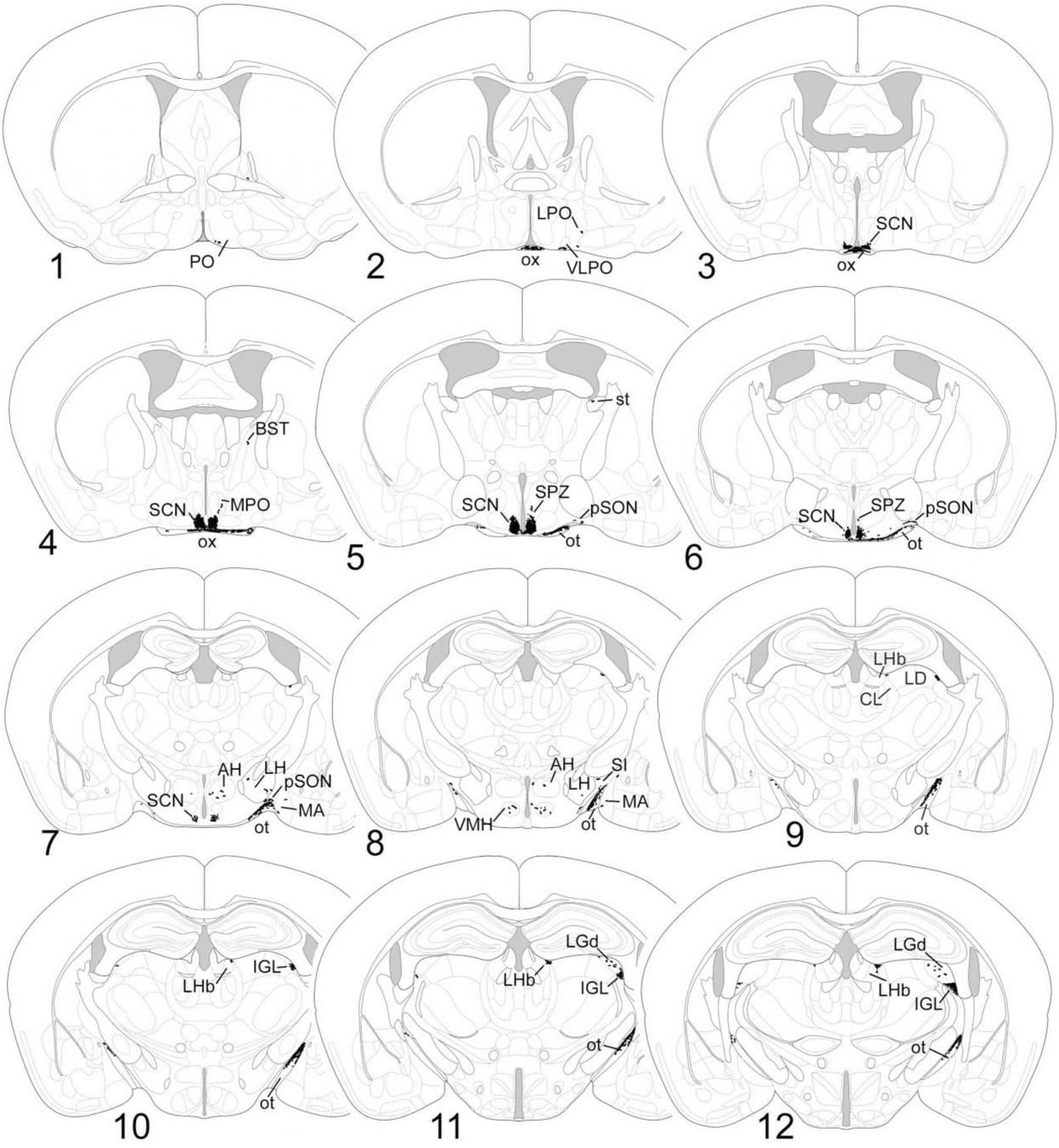

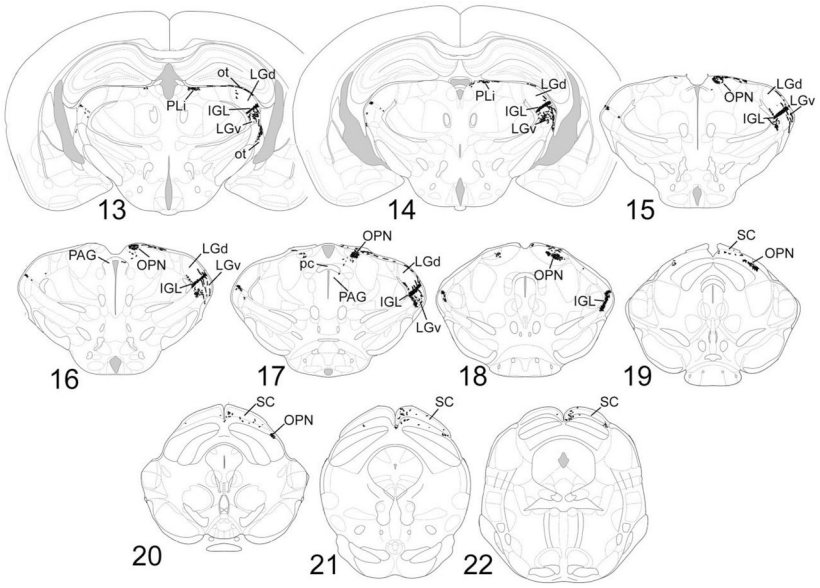

Fig. 4.

1–22: Chartings of schematic coronal sections, modified from the atlas of Paxinos and Franklin (2001), summarizing the distribution of X-gal-labeled fibers as seen in cases of monocular enucleation. The right side of the brain, shown on the right of each charting, is contralateral to the intact eye. For abbreviations, see list.

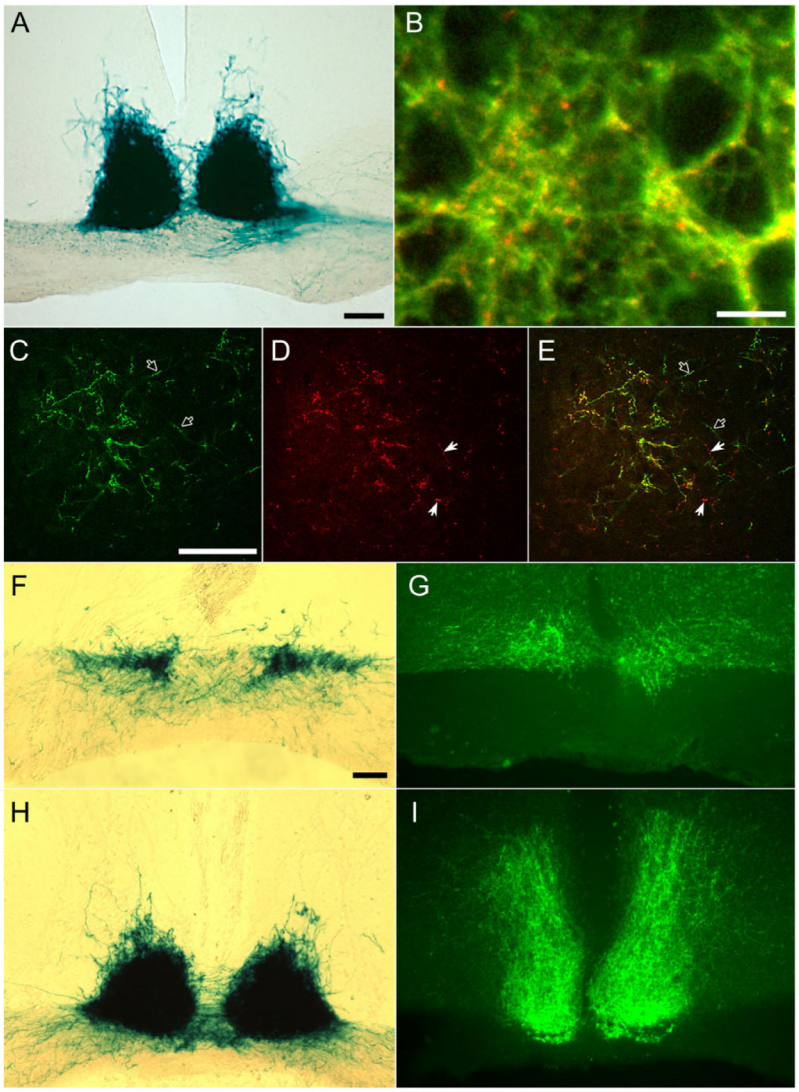

Fig. 5.

Axonal terminations of melanopsin ganglion cells in the suprachiasmatic nucleus of the hypothalamus. **A:** X-gal staining of melanopsin afferents to the SCN after right monocular enucleation. Although most labeled fibers in the contralateral (left) optic tract have degenerated, leaving only weak, granular labeling, labeling of the SCN is bilaterally symmetric. **B:** Confocal image of SCN showing double immunostaining for all contralateral retinal inputs (red; anti-cholera toxin B [CTB] immunofluorescence) and for all bilateral melanopsin RGC inputs (green; anti-β-galactosidase immunofluorescence). Most red, CTB-labeled afferents exhibit green anti-β-galactosidase labeling also, giving them a yellow appearance in the image, but a few contain little if any green labeling and presumably arise from non-melanopsin RGCs. Green axons lacking red immunofluorescence are presumably melanopsin afferents from the ipsilateral eye, which was not injected with CTB. Large circular dark profiles are unlabeled somata of SCN neurons. Projected stack of seven 1-μm confocal optical sections. **C–E:** Confocal image (optic section thickness 1 μm) grazing the caudal margin of the SCN from the same brain as in B and labeled by the same double-immunofluorescence method. Reduced afferent density permits individual axons to be resolved. Filled arrows indicate crossed retinal afferents (red) that are β-galactosidase negative (no green). Open arrows denote presumptive

ipsilateral afferents from melanopsin RGCs (green, no red). **F–I:** Comparison of the distribution within the SCN and vSPZ of axons of melanopsin ganglion cells (X-gal staining in F and H) with those of VIP-immunoreactive processes in serially adjacent sections. F and G are from the rostral pole of the SCN; H and I are from the mid-caudal SCN. Wisps of fiber labeling dorsal to the main SCN field in H lie within the vSPZ. Scale bar = 100 μm in A, C (applies to C–E), and F (applies to F–I); 10 μm in B.

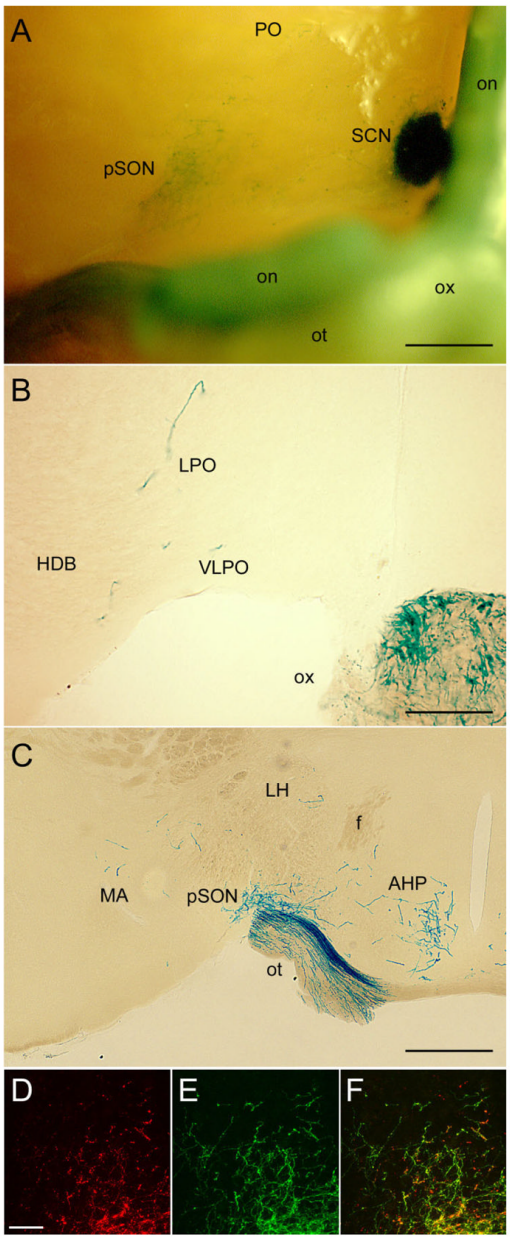

Fig. 6.

Hypothalamic and other basal limbic targets beyond the SCN. **A:** Basal view of X-gal-stained whole brain. Top of image is rostral and the right margin is near the midline. The optic chiasm and the right optic nerve and tract (left in image) have been retracted caudally to expose the right SCN and pSON. A few fibers are also evident in the preoptic region. **B,C:** X-gal staining in coronal sections just rostral (B) or caudal (C) to the SCN, showing scattered fibers in the preoptic area including the VLPO (B), dense input to the peri-SON (C), and scattered labeling in the anterior and lateral hypothalamus and medial amygdala (C). **D–F:** Confocal immunofluorescence images of the ventral SPZ illustrating relationship between crossed retinal afferents (red; D) and afferents from melanopsin RGCs (green, E). Format as in Figure 5C–E; F is the merged image. Many but not all of the crossed retinal afferents arise from β-galactosidase-positive (melanopsin) afferents. For abbreviations, see list. Scale bar = 500 μm in A and C; 200 μm in B; 25 μm in D (applies to D–F).

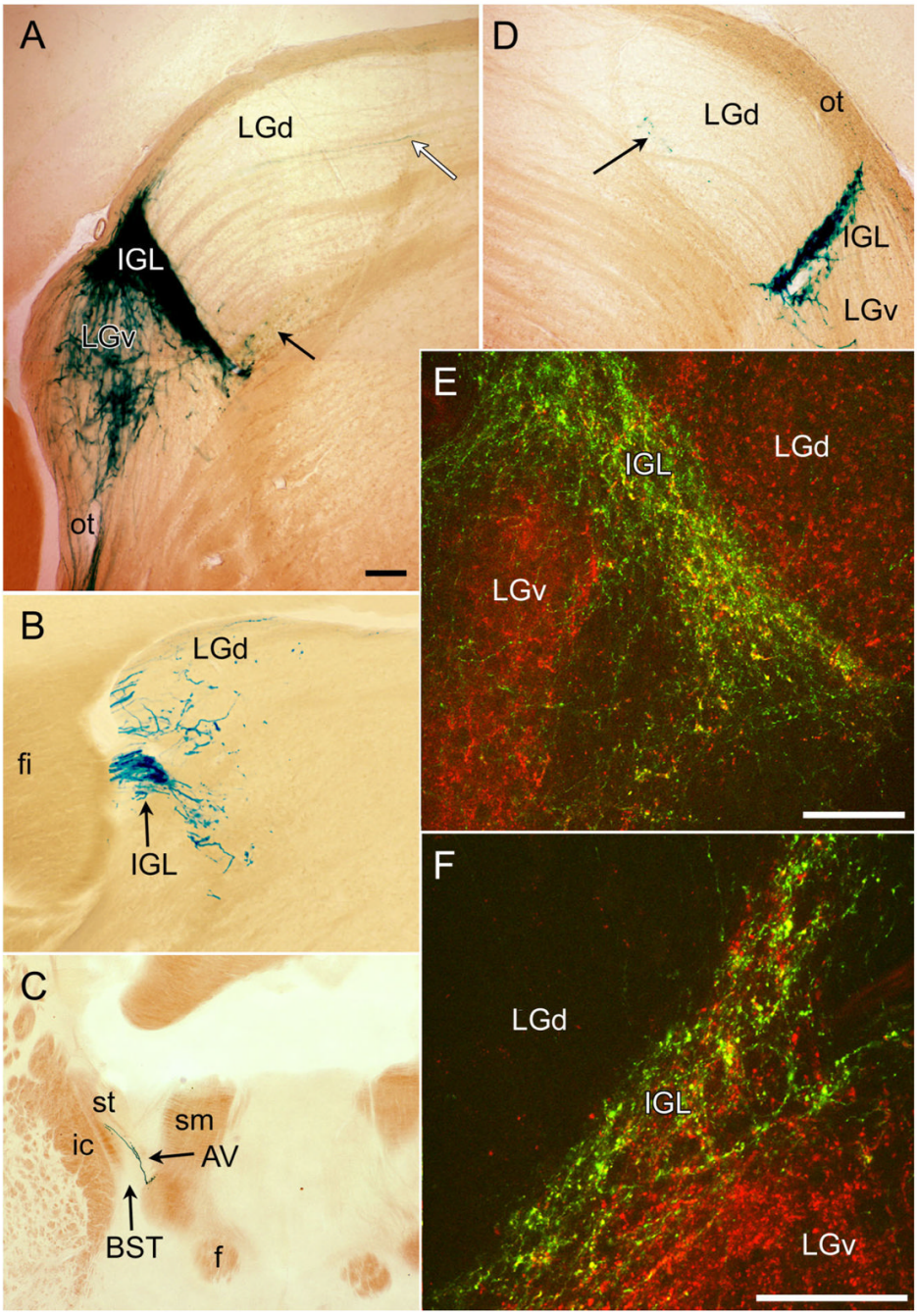

Fig. 7.

Distribution of afferents from melanopsin ganglion cells in lateral geniculate complex. **A–D:** Coronal sections reacted with X-gal. A and D are from middle of rostrocaudal extent of LGd. A is contralateral and D is ipsilateral to the remaining eye in a monocularly enucleated mouse. Black arrows indicate sparse terminal labeling near the ventromedial margin of LGd. White arrow in A indicates axon of passage in one of the fascicles traversing the LGd. B shows substantial terminal labeling at the rostral margin of the LGd as well as strong labeling of the IGL at this level. C shows the rostral limit of this terminal field in or near the BST. **E,F:** Confocal merged immunofluorescence images of the IGL and adjacent geniculate nuclei illustrating relationship between afferents from mRGCs of both eyes (green) and total retinal

afferents (red) from one eye, either the contralateral eye (E) or the ipsilateral eye (F). Most retinal afferents to the IGL are from melanopsin RGCs (green and yellow puncta), but many are not (red puncta). Green profiles (without red) represent terminations of axons from mRGCs in the eye not injected with CTB. Most retinal afferents to the LGv do not arise from melanopsin RGCs. For abbreviations, see list. Scale bar = 100 μm in A–F.

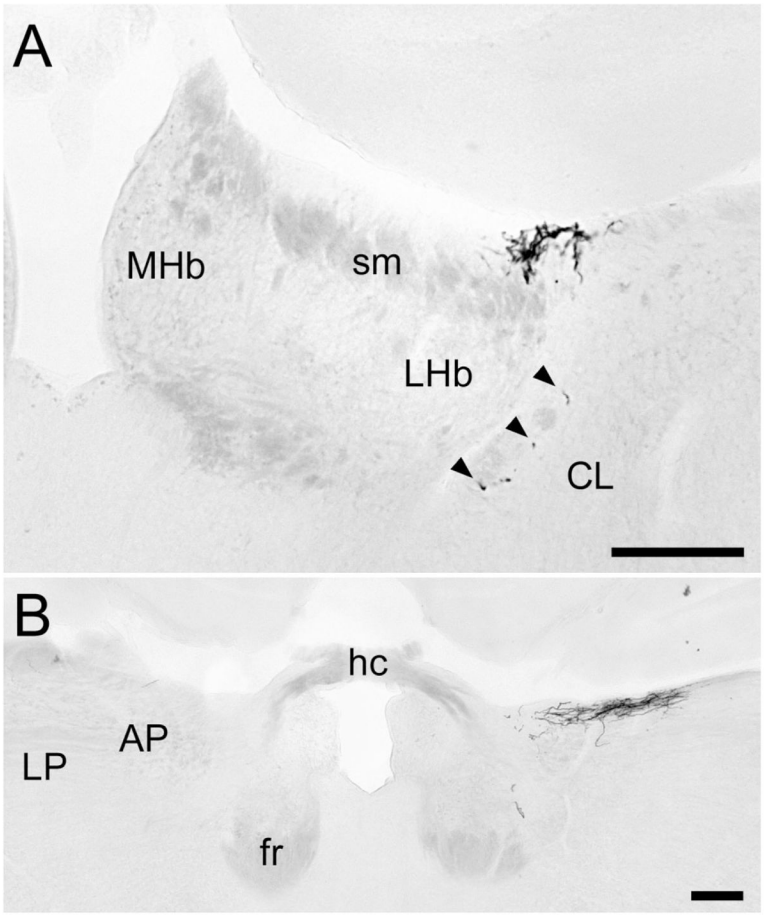

Fig. 8.

X-gal-stained coronal sections illustrating inputs to the region of the habenula and posterior limitans nucleus. **A:** Mid-habenular level; midline is at the left edge of the image. The main terminal field lies at dorsolateral margin of the stria medullaris and lateral habenula, with scattered fibers (arrowheads) within the fiber capsule bounding the habenular complex ventrolaterally. **B:** The caudal end of the terminal field, at the level of the habenular commissure. The plexus of labeled fibers on the right lies at the dorsal surface near the boundary of the midbrain (represented by the anterior pretectal nucleus) and the thalamus (represented by the lateral posterior nucleus), in a region included within the posterior limitans nucleus in other rodents. The right eye was enucleated in this animal, leading to nearly complete loss of labeled axons on the left. For abbreviations, see list. Scale bar = 200 μm in A,B.

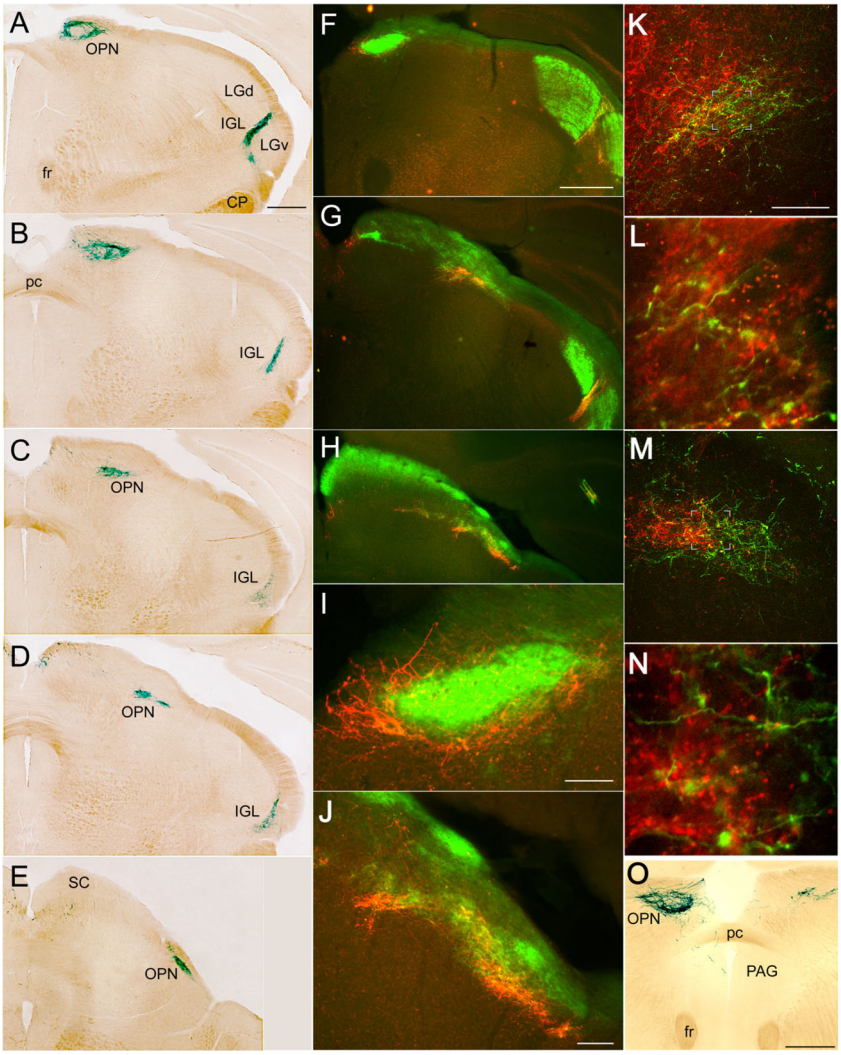

Fig. 9.

Distribution of afferents from melanopsin ganglion cells within the olivary pretectal nucleus (OPN), caudal IGL, and periaqueductal grey. **A–E:** Coronal series through the OPN stained with X-gal; section A is most rostral. **F–J:** Double-immunofluorescence micrographs of coronal sections illustrating relationship of afferents from melanopsin ganglion cells (red anti-β-galactosidase) with overall crossed retinal input (green CTB). F, G, and H are at roughly the same level as A, C, and D, respectively. I and J are higher power views of F and H, respectively. **K,L:** Confocal merged double-immunofluorescence images of the left OPN and adjacent pretectal nuclei illustrating the relationship between afferents from melanopsin RGCs (green; anti-β-galactosidase) and contralateral retinal afferents (red; anti-CTB; note that assignment of fluorophores is reversed from that in F–J). L is an enlarged, higher resolution scan of the boxed area in K. Note that the OPN, as defined by input from melanopsin afferents, is a small part of a much larger field of crossed retinal input (K). In L, most melanopsin afferents in the OPN contain anterograde label transported from the contralateral eye (green + red = yellow), but the terminal at the bottom right lacks red anti-CTB labeling and presumably arises from the ipsilateral eye. **M,N:** The same as K and L, but from the other side of the brain (right), so that anterograde CTB label (red) marks inputs from the ipsilateral eye. N is enlarged from the boxed region in M. In M, note the modest overlap between the field of melanopsin afferents

(green) and the patch of uncrossed retinal input (red). Most melanopsin afferents in N lack anterograde label, presumably because they come from the contralateral eye. Within the OPN as defined by the melanopsin afferent terminal field, many retinal afferents, both crossed (K,L) and uncrossed (M,N), lack β-galactosidase (red +, green −) and thus presumably arise from non-melanopsin ganglion cells. **O:** Coronal section through the OPN stained with X-gal after enucleation of the left eye. Note the pronounced reduction in the labeled terminal field contralateral to the enucleation (right). On the left, fibers descending from the OPN penetrate the posterior commissure (pc) to enter the periaqueductal gray (PAG). For abbreviations, see list. Scale bar = 500 μm in A (applies to A–E), F (applies to F–H), and O; 200 μm in K (applies to K–M); 100 μm in I,J.

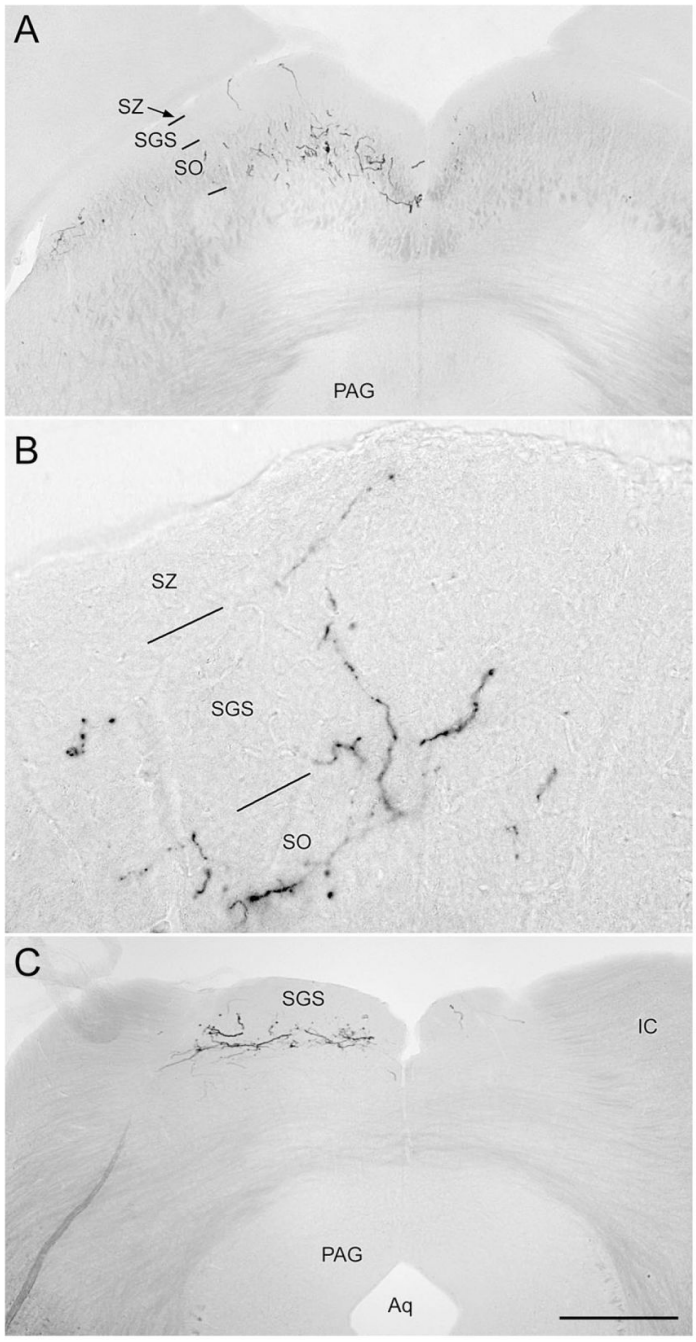

Fig. 10.

Coronal sections illustrating X-gal staining of melanopsin afferents to the superior colliculus. The left eye was enucleated, leaving only right-eye afferents intact. **A:** Rostral superior colliculus. Fiber labeling is heaviest in the stratum opticum (SO), especially medially and laterally, but some fibers invade the stratum griseum superficiale (SGS) and stratum zonale (SZ). **B:** Higher magnification view of left colliculus in a similar section from a different brain. **C:** Caudal pole of superior colliculus, from the same brain as shown in A. In A and C, a few melanopsin afferents from the ipsilateral eye are apparent in the right colliculus. For abbreviations, see list. Scale bar in C = 500 μm in A,C and 200 μm in B.